Performance Analysis and Optimization for Jammer-Aided Multi-Antenna UAV Covert Communication

Hongyang Du, Dusit Niyato, *Fellow, IEEE*, Yuan-ai Xie, Yanyu Cheng, Jiawen Kang*, and Dong In Kim, *Fellow, IEEE*

Abstract—Unmanned aerial vehicles (UAVs) have attracted a lot of research attention because of their high mobility and low cost in serving as temporary aerial base stations (BSs) and providing high data rates for next-generation communication networks. To protect user privacy while avoiding detection by a warden, we investigate a jammer-aided UAV covert communication system, which aims to maximize the user's covert rate with optimized transmit and jamming power. The UAV is equipped with multi-antennas to serve multi-users simultaneously and enhance the Quality of Service. By considering the general composite fading and shadowing channel models, we derive the exact probability density (PDF) and cumulative distribution functions (CDF) of the signal-to-interference-plus-noise ratio (SINR). The obtained PDF and CDF are used to derive the closed-form expressions for detection error probability and covert rate. Furthermore, the covert rate maximization problem is formulated as a Nash bargaining game, and the Nash bargaining solution (NBS) is introduced to investigate the negotiation among users. To solve the NBS, we propose two algorithms, i.e., particle swarm optimization-based and joint two-stage power allocation algorithms, to achieve covertness and high data rates under the warden's optimal detection threshold. All formulated problems are proven to be convex, and the complexity is analyzed. The numerical results are presented to verify the theoretical performance analysis and show the effectiveness and success of achieving the covert communication of our algorithms.

Index Terms—Covert communication, multi-antenna UAV, performance analysis, optimization, Bargaining game.

I. INTRODUCTION

Wireless communication networks have always required a high data rate and secure transmission. As sixth-generation networks aspire for higher capacity, lower latency, and higher user density, the number of mobile users and devices is rapidly rising, which poses great challenges in the near-future development of Internet-of-things (IoT). In remote areas without terrestrial infrastructures and disaster-affected areas with damaged infrastructures, efficient communication service for ground users and devices cannot be guaranteed. Furthermore, since each IoT device has a restricted transmission range, the signal cannot travel a long distance. Due to these limitations, common ground base stations (BSs) may be unable to cover all IoT devices and gather data effectively. As a result, a new paradigm is urgently required to enhance the cellular network's quality of service (QoS).

Because of the flexible operation and large coverage [1], unmanned aerial vehicle (UAV)-aided communications are regarded as one of the most promising techniques for future networks [2], [3]. By acting as temporary aerial BSs, UAVs can perform a broad range of activities, including disaster rescue support, real-time surveillance, and data collection [4], [5]. To meet the ever-increasing demands, it is potential to adopt multi-antennas at the UAV to improve the channel quality [6]. The multi-antenna access and high mobility of the UAV improve the system performance significantly, but several challenges remain. For example, because of the wide coverage and large-scale connection provided by UAVs, open networks are susceptible to eavesdropping and various attacks by malicious adversaries [7], [8]. Since UAVs are commonly used to transmit private data, it is critical to design a secure UAV-aided system [9]–[12].

Several related works consider enhancing the security of UAV networks [5], [13]–[15], which can be divided into two major categories, i.e., cryptographic methods [13], [14] and physical layer security techniques [4], [5], [15]. However, several practical situations require not only the security of the transmitted content but also the covertness of the transmission behavior, which has not been addressed and is also desirable

H. Du is with the School of Computer Science and Engineering, the Energy Research Institute @ NTU, Interdisciplinary Graduate Program, Nanyang Technological University, Singapore (e-mail: hongyang001@e.ntu.edu.sg).

D. Niyato is with the School of Computer Science and Engineering, Nanyang Technological University, Singapore (e-mail: dniyato@ntu.edu.sg)

Yuan-ai Xie is with the Institute of Electrical Engineering, Yanshan University, Qinhuangdao 066004, China. (emails: xieyuan_ai@163.com)

Y. Cheng is with Alibaba-NTU Singapore Joint Research Institute, Nanyang Technological University, Singapore 639798 (e-mail: yanyu.cheng@ntu.edu.sg).

J. Kang is with the School of Automation, Guangdong University of Technology, China. (e-mail: kavinkang@gdut.edu.cn)

D. I. Kim is with the Department of Electrical and Computer Engineering, Sungkyunkwan University, Suwon 16419, South Korea (e-mail: dikim@skku.ac.kr)

TABLE I
A COMPARISON OF CONTRIBUTION BETWEEN RELEVANT SURVEYS AND OUR SURVEY.

Reference	Key contributions of the survey	How our survey differs
[?]	A vision paper whose goal is to motivate a paradigm shift from the mainstream research. Discuss the importance of SemCom and suggest a new architecture that facilitates an efficient cross-layer design capitalizing on the new levels.	We present a comprehensive analysis of current technical papers that apply SemCom in the latest 6G networks, and detail the features of SemCom and 6G.
[?]	Introduce the SemCom principles and two design approaches, i.e., layer-coupling design and end-to-end design using a neural network. Discuss specific techniques for different application areas of SemCom.	We classify the SemCom into three categories, which is more complete and covers the various ways how the SemCom is currently applied in 6G. The future research directions can also be inspired by our classification.
[?]	Review classic semantic communication frameworks and then propose an architecture based on federated edge intelligence for supporting resource-efficient semantic-aware networking.	Not comprehensive
[?]	Apply SemCom to a communication scenario where the destination is tasked with real-time source reconstruction for the purpose of remote actuation.	Not comprehensive
[?]	An overview of the latest deep learning (DL) and end-to-end (E2E) communication based SemCom is given and open issues that need to be tackled is discussed explicitly.	Not comprehensive

for UAV networks. The reason is that once the transmission behavior of a transmitter is detected by malicious users, its location information is exposed, which makes the transmitter vulnerable to physical attacks [16]. Fortunately, the emerging covert communication technique can effectively hide the existence of a wireless transmission, i.e., avoiding a wireless transmission being detected by the adversary, called warden.

Existing works indicate that covert communication can be achieved through random noises [17] or interference [12]. To degrade the detection performance of the warden, a friendly jammer is introduced to assist the communication by actively generating jamming signals. Unlike the random noise behaving uncontrollably, the interference can be controlled effectively by optimizing the jammer's power. Nevertheless, subject to the power constraint and the minimum covert-rate requirement of users, the friendly jammer aims to use less power to help each user achieve a higher covertness. The contradicted and independent individual objectives of user-jamming antenna pairs impel us to study how users bargain and negotiate with each other to achieve their covert communication. Hence, it is natural to apply game theory to balance the objectives among different pairs [18]–[20]. Accordingly, to design the transmit and jamming power allocation and achieve the optimal secure UAV-aided communication, a Nash bargaining approach is proposed to obtain the Nash bargaining solution (NBS) [21]. Thus, an agreement can be achieved by players, i.e., K users, efficiently and fairly, given the NBS's five axioms of pareto optimality (PAR), individual rationality (IR), independent of expected utility representations (INV), independence of irrelevant alternatives (IIA) and symmetry (SYM) [21].

In this paper, we adopt two more practical and accurate channel models, namely Fisher–Snedecor $\mathcal{F}$ [22] and Fluctuating Two-Ray (FTR) models [23], than traditional Nakagami-m [24] and Rician models [25] to conduct a detailed performance analysis about the jammer-aided multi-antenna UAV covert communication system. Based on the obtained analytical results, bargaining game theory is used to determine the optimal transmit and jamming power allocation scheme. The main contributions are summarized as follows:

- We investigate a jammer-aided multi-antenna UAV covert communication system. By modeling the ground channel links as Fisher-Snedecor $\mathcal{F}$ fading and the air-to-ground channel links as FTR fading, the exact probability density function (PDF) and cumulative distribution function (CDF) of the end-to-end signal-to-interference-plus-noise ratio (SINR) are derived. To the best of our knowledge, this is the first study that analyzes a jammer-aided UAV covert communication system over composite fading and shadowing with accurate and tractable generalized channel models.
- The closed-form expressions for the detection error probability and covert rate are derived. To maximize the user's covert rate with limited transmit and jamming power, the optimization problem is formulated as a Nash bargaining game (NBG) with the help of the derived performance metrics. Furthermore, the NBS is introduced to investigate the transmit and jamming power resource negotiation among the players, i.e., users in multi-antenna UAV-aided covert communication networks, to reach an agreement that is efficient and fair. Moreover, with the help of characteristics of generalized hypergeometric functions, we investigate the optimization problem's convergence based on analytical expressions. The convergences of all problems formulated in this paper are proven, and the complexity is formally analyzed.
- We propose two algorithms, i.e., particle swarm optimization (PSO)-based power allocation (PPA) and joint two-stage power allocation (JTPA) algorithms, to solve the formulated problem. To demonstrate the robustness of the proposed algorithms, we assume that the warden can find the optimal detection threshold, i.e., the warden can do the most harm to the covertness. A detection error probability minimization algorithm for the warden is also presented. In the proof of convergence, we study

an integral equation that has not been analyzed in any function books, e.g., [26]–[28]. The obtained results and approximations are useful in the performance analysis of wireless communications systems.

The remainder of the paper is organized as follows: In Section II, we introduce the jammer-aided multi-antenna UAV covert communication, and derive exact statistics for the end-to-end SINR. In Section III, closed-form performance metrics, such as detection error probability and covert rate, are derived. With help of the derived metrics and bargaining game theory, we formulate the optimization problem as a NBG to maximize the user's covert rate in Section IV. Section V presents the PPA and JTPA algorithms. Numerical results and Monte-Carlo simulations are presented in Section VI to verify the accuracy of our analysis and proposed power allocation algorithms. Finally, Section VII concludes this paper.
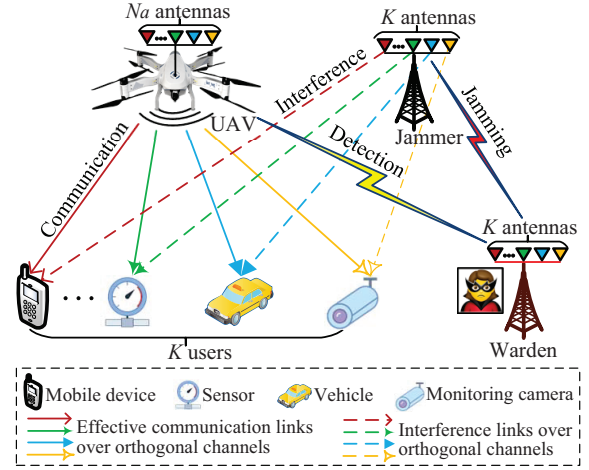

Fig. 1. A jammer-aided multi-antenna UAV covert communication system.

TABLE II
MATHEMATICAL NOTATIONS AND FUNCTIONS

$\Pr\{\cdot\}$	Probability function
$\boldsymbol{a}^T$	Transpose of vector $\boldsymbol{a}$
K	The average power ratio of the dominant wave to the scattering multipath in FTR fading model
m_k, m_w	The fading severity parameter for the k_{th} user & warden in FTR fading model
Δ_k, Δ_w	A parameter varying from 0 to 1 representing the similarity of two dominant waves for the k_{th} user & warden in FTR fading model
σ_k, σ_w	The standard deviation of the diffuse received signal component for the k_{th} user & warden in FTR fading model
υ_k, υ_w	The received average SNR for the k_{th} user & warden in FTR fading model, and $\upsilon = 2\sigma^2(1+K)$
m_{fk}, m_{fw}	The fading parameters for the k_{th} user & warden in Fisher-Snedecor $\mathcal{F}$ fading model
m_{sk}, m_{sw}	The shadowing parameters for the k_{th} user & warden in Fisher-Snedecor $\mathcal{F}$ fading model
$\bar{z}_k$, $\bar{z}_w$	The average value of $\mathcal{F}$ random variables (RVs), i.e., z, for the k_{th} user & warden in Fisher-Snedecor $\mathcal{F}$ fading model
$_1F_1(\cdot;\cdot;\cdot)$	Confluent hypergeometric function [27, eq. (9.210.1)]
$\Gamma(z)$	Gamma function [27, eq. (8.310.1)]
$\gamma(\cdot,\cdot)$	Incomplete gamma function [27, eq. (8.350.1)]
$B(\cdot,\cdot)$	Beta function [27, eq. (8.384.1)]
$_2F_1(\cdot,\cdot;\cdot;\cdot)$	Gauss hypergeometric function [27, eq. (9.111)]
$H_{\cdot\cdot}^{\cdot\cdot}(\cdot|\cdot)$	Multivariate Fox's H-function [29, eq. (A-1)]

II. SYSTEM MODEL AND SINR ANALYSIS

A. System Description

As shown in Fig. 1, we consider a jammer-aided multi-antenna UAV covert communication network. The UAV collects private data, such as surveillance images and users' travel trajectories, for K users. Now, the UAV is transmitting the users' different data to the corresponding users simultaneously with the help of multi-antennas. Note that these users could be mobile devices, vehicles, or sensors. To prevent private

data transmission from being detected by a malicious warden, a friendly jammer is used to improve the covertness of communication.

Specifically, we assume that all users are equipped with a single antenna. Every user wants to improve its QoS, which includes data transmission and covertness, by purchasing UAV's transmitting power and jammer's jamming power. To avoid the interference among users, the UAV assigns different orthogonal frequency channels to use the k_{th} antenna to serve k_{th} user individually. Because the channel assignment information can be shared with the friendly jammer to facilitate covert communication, the jammer uses its k_{th} antenna to jam the k_{th} channel to interfere the warden's detection. However, the jamming signals also have a negative impact on the user's SINR. We adopt a three-dimensional Cartesian coordinate system to represent the location. The locations of the user U_k, the jammer, the UAV, and the warden can be expressed by $\mathbf{q}_k = [x_k, y_k, z_k]^T$ $(\forall k \in \mathcal{K})$, $\mathbf{q}_j = [x_j, y_j, z_j]^T$, $\mathbf{q}_a = [x_a, y_a, z_a]^T$ and $\mathbf{q}_w = [x_w, y_w, , z_w]^T$, respectively. Therefore, the distances of the air-to-ground links, i.e., from UAV to the user U_k and the warden, can be expressed as D_{ak} and D_{aw}, respectively, where $D_{ai} = \|\mathbf{q}_a - \mathbf{q}_i\|$ $(i = k, w)$. The distances of the ground-to-ground links from the jammer to the kth user and the warden are denoted by D_{jk} and D_{jw}, respectively, where $D_{ji} = \|\mathbf{q}_j - \mathbf{q}_i\|$.

Remark 1. *Because we use the generalized fading models with mathematical analysis complexity, our performance metrics are derived based on the scenario where one user is served by one antenna to reduce the complexity and obtain more insights. Note that our analysis can be generalized to the case of multi-antennas serving one user by a simple transformation [30], i.e., the UAV uses N_k antennas to serve the user U_k and $\sum_{k=1}^{K} N_k = N_a$. The reason is that we use FTR fading to model the small-scale fading in air-to-ground links (see Section II-B2), and the single FTR distribution can be regarded as the approximation to the distribution of the sum of FTR RVs [30], i.e., if $N_k \sim FTR\left(m_k, K_k, \sigma_k^2, \Delta_k\right),$*

we have $\sum_{k=1}^{K} N_k \sim FTR\left(\tilde{m}, \tilde{K}, \tilde{\sigma}^2, \tilde{\Delta}\right)$. *The parameters* $\left\{\tilde{m}, \tilde{K}, \tilde{\sigma}^2, \tilde{\Delta}\right\}$ *can be obtained easily [30]. A detailed analysis on transmit beamforming via the precoding associated with each user data, when K_i antennas at UAV are used to serve one user, will be left for the future work.*

B. Channel Model

Consider a large-scale and small-scale composite channel model. It is worth noting that air-to-ground and ground-to-ground connections could have various path loss exponents and thus require different fading models. The reason is that air-to-ground links have less obstruction, resulting in a much more stable line-of-sight (LoS) path. However, the ground environment in which the users, jammer, and warden are located, is typically dynamic, which may cause larger path loss exponents and composite fading and shadowing. In the following, we propose the path loss model and the small scale model for the air-to-ground links and the ground-to-ground links, respectively.

1) Path Loss Model: To simulate the air-to-ground and ground-to-ground links, different path loss coefficients are used, which are given as [31]

$$L\left(d\right) = \begin{cases} D_{ai}^{-\alpha_{ai}}, & \text{for air-to-ground links,} \\ D_{ji}^{-\alpha_{ji}}, & \text{for ground-to-ground links,} \end{cases} \quad (1)$$

where α_{ai} $(i \in \{k, w\})$ denotes the path loss exponents of the UAV-user U_k link and the UAV-Warden link, respectively, and α_{ji} $(i = k, w)$ are the path loss exponents of the Jammer-user U_k link and the Jammer-Warden link. Typical values of α can be defined in [31, Table 1], while $\alpha_{ai} < \alpha_{ji}$ holds in general.

2) Small-Scale Model: To unify system performance with various channel environments, generalized fading distributions are proposed, which include the most other fading distributions as special cases [32], [33]. In the following, we introduce the fluctuating two-ray (FTR) and Fisher-Snedecor $\mathcal{F}$ fading distributions to model the air-to-ground and ground-to-ground links, respectively. The reason is as follows:

- The FTR fading model [34] is a generalization of the two-wave with diffuse power fading model, which allows the constant amplitude specular waves of LoS propagation to fluctuate randomly. Recent small-scale fading measurements of the 28 GHz outdoor millimeter-wave channels [34] have shown that the FTR fading can provide a significantly better match to the real channel than the Rician fading. Therefore, we utilize the FTR fading model to illustrate the channel coefficients between the UAV and the user U_k or warden, which have less obstruction, resulting in a much more stable LoS path.
- To create a realistic ground link model, we assume that each ground connection's small-scale fading follows Fisher-Snedecor $\mathcal{F}$ fading distribution, which has been proven to give a more thorough modeling and characterization of the simultaneous occurrence of multipath fading and shadowing [22]. In addition, the Fisher-Snedecor $\mathcal{F}$ model is more generic and covers several fading distributions as special cases, as well as being

more mathematically tractable. For example, when the parameter m_s tends to be infinity, the Fisher-Snedecor $\mathcal{F}$ distribution becomes the Nakagami-m distribution. Moreover, special cases of Fisher-Snedecor $\mathcal{F}$ includes Rayleigh ($m = 1$) and one-sided Gaussian ($m = 1/2$).

Let $X \sim FTR\left(m, K, \sigma^2, \Delta\right)$. The PDF and CDF of the squared FTR RV X can be expressed, respectively, as follows [23]:

$$f_X(x) = \frac{m^m}{\Gamma(m)} \sum_{j=0}^{M} \frac{K^j \alpha_j}{j!} \frac{x^j}{\Gamma(j+1)(2\sigma^2)^{j+1}} \exp\left(-\frac{x}{2\sigma^2}\right), \quad (2)$$

$$F_X(x) = \frac{m^m}{\Gamma(m)} \sum_{j=0}^{M} \frac{K^j \alpha_j}{j!} \frac{1}{\Gamma(j+1)} \gamma\left(j+1, \frac{x}{2\sigma^2}\right), \quad (3)$$

where

$$\alpha_j = \sum_{k=0}^{j} \binom{j}{k} \sum_{l=0}^{k} \binom{k}{l} \Gamma(j+m+2l-k)(m+K)^{k-j-m-2l}$$
$$\times K^{2l-k} \left(\frac{\Delta}{2}\right)^{2l} (-1)^{2l-k} R_{j+m}^{k-2l} \left(\left(\frac{K\Delta}{m+K}\right)^2\right), \quad (4)$$

$$R_v^\mu(x) = \begin{cases} \frac{(v-\mu)}{2} \frac{(v-\mu+1)}{2} \frac{x^\mu}{\mu!} {}_2F_1\left(\frac{v+\mu}{2}, \frac{v+\mu+1}{2}; 1+\mu; x\right), \mu \in N, \\ \frac{{}_2F_1\left(\frac{v-\mu}{2}, \frac{v-\mu+1}{2}; 1-\mu; x\right)}{\Gamma(1-\mu)}, \text{otherwise,} \end{cases} \quad (5)$$

and M is a large constant that satisfies $\sum_{j=0}^{M} \alpha_j \to 1$. Typically, to obtain a satisfactory accuracy, e.g., $1 - \sum_{j=0}^{M} \alpha_j < 10^{-6}$, only less than 30 terms are needed [35], which is easy to compute.

Let $Z \sim \mathcal{F}(m_f, m_s, \bar{z})$, the PDF and CDF of the squared $\mathcal{F}$ RV Z can be written as [36]

$$f_Z(z) = \frac{m_f^{m_f}(m_s-1)^{m_s} \bar{z}^{m_s} z^{m_f-1}}{B(m_f, m_s)(m_f z + (m_s-1)\bar{z})^{m_f+m_s}}, \quad (6)$$

and

$$F_Z(z) = \frac{m_f^{m_f-1} z^{m_f}}{B(m_f, m_s)(m_s-1)^{m_f} \bar{z}^{m_f}}$$
$$\times {}_2F_1\left(m_f, m_f+m_s, m_f+1; -\frac{m_f z}{(m_s-1)\bar{z}}\right). \quad (7)$$

With the above accurate modeling of the channels, we can further analyze the SINR of the system and derive the PDF and CDF expressions in the following.

C. SINR Analysis

We consider K users using different time-frequency resource blocks, which corresponds to the practical scenario when orthogonal multiple access is used [37]. K antennas in UAV are used to serve K users for tractable analysis under the generalized composite model of large-scale and small-scale fading channels. Therefore, the signal received by the user U_k can be expressed as

$$y_k = \sqrt{D_{ak}^{-\alpha_{ak}} P_{ak}} h_{ak} s_k + n + \sqrt{D_{jk}^{-\alpha_{jk}} P_{jk}} h_{jk}, \quad (8)$$

where P_{ak} denotes the transmit power of the antenna which operates on the k_{th} channel, h_{ak} is the channel coefficient of the air-to-ground link from UAV to user U_k, s_k denotes the private data of user U_k, $\|s_k\|^2 = 1$, P_{jk} denotes the jamming power allocated to user U_k, h_{jk} is the channel

coefficient of the ground link form jammer to user U_k, and n is the additive white Gaussian noise (AWGN) at the user with $n \sim \mathcal{CN}\left(0, \kappa^2\right)$. We denote the maximal sum transmit power of UAV by P_T. Hence, the transmit power constraint can be formulated as $\sum_{k=1}^{K} P_{ak} \leq P_T$. Similarly, let P_J denote the total jamming power, we have $\sum_{k=1}^{K} P_{jk} \leq P_J$.

With the help of (8), the SINR of user U_k can be expressed as

$$\gamma_k = \frac{D_{ak}^{-\alpha_{ak}} P_{ak} h_{ak}^2}{\kappa^2 + D_{jk}^{-\alpha_{jk}} P_{jk} h_{jk}^2} \triangleq \frac{C_{1k} X_k}{\kappa^2 + C_{2k} Z_k}, \quad (9)$$

where $X_k \triangleq h_{ak}^2 \sim FTR\left(m_k, K_k, \sigma^2_k, \Delta_k\right)$, $Z_k \triangleq h_{jk}^2 \sim \mathcal{F}\left(m_{fk}, m_{sk}, \bar{z}_k\right)$, $C_{1k} \triangleq D_{ak}^{-\alpha_{ak}} P_{ak}$, and $C_{2k} \triangleq D_{jk}^{-\alpha_{jk}} P_{jk}$.

Next, we derive the PDF and CDF of γ_k to further analyze the covert performance and provide a basis for the design of joint transmit power and jamming power allocation scheme.

III. Covert Performance Metrics and Analysis

A. Statistical Expressions and Approximations

1) Statistical Expressions: To perform the performance analysis of the system, the PDF and CDF expressions should be derived, which are presented in the following lemma.

Lemma 1. *The PDF and CDF of the k-th user's SINR can be derived as* (10) *and* (11), *respectively, shown at the bottom of the next page, where $\Omega_k \triangleq \left(m_{sk} - 1\right) \bar{z}_k C_{2k}$.*

Proof: Please refer to Appendix A. ∎

In the following, we analyze truncation errors to demonstrate how infinite series affect the performance of the CDF expression. The truncation error of the $F_{\gamma_k}(\gamma)$ with respect to the first M terms is given by [38, eq. (32)]

$$\varepsilon\left(M\right) \triangleq F_Y(\infty) - \hat{F}_Y(\infty). \quad (12)$$

Table III illustrates the required truncation terms M for different channel parameters to demonstrate the convergence of the series in (12). We can observe that only less than 30 terms are necessary for all considered cases with a desired accuracy of 10^{-5} or less.

2) Approximations Analysis: Although the previously derived analytical results have been obtained in closed-form, they may not provide many insights as to the factors affecting system performance. In the following, we analyze asymptotic performance that becomes tight in the high-SNDR or high-L regime.

TABLE III
Minimum Required Terms and Truncation Error for Different Parameters with $K_k = 10$, $\Delta_k = 0.3$, $m_{sk} = 2$, $\bar{z} = 20$, $D_{ak} = D_{jk} = 10$, $\alpha_{ak} = \alpha_{jk} = 2$, $P_{jk} = 10$, and $\kappa^2 = 1$.

Parameter	$\varepsilon\left(L\right)$	M
$m_k = 4$, $m_{fk} = 3$, $P_{ak} = 13$, $\sigma^2{}_k = 0.2$	7.34×10^{-6}	21
$m_k = 5$, $m_{fk} = 5$, $P_{ak} = 16$, $\sigma^2{}_k = 0.5$	8.93×10^{-6}	24
$m_k = 7$, $m_{fk} = 8$, $P_{ak} = 26$, $\sigma^2{}_k = 0.3$	8.58×10^{-6}	19
$m_k = 2$, $m_{fk} = 4$, $P_{ak} = 14$, $\sigma^2{}_k = 0.7$	7.02×10^{-6}	22

Proposition 1. *When the jamming signal has weak interference to the receiver, i.e., the kth user, the CDF of γ_k can be approximated as*

$$F_{\gamma_k}^{\mathrm{LJ}}(\gamma) = \frac{m_k^{m_k}}{\Gamma\left(m_k\right)} \left(\frac{m_{fk}\kappa^2}{m_{fk}\kappa^2 - \Omega_k}\right)^{m_{fk}}$$
$$\times \sum_{j=0}^{M} \frac{K_k^j \alpha_{kj}}{\Gamma(j+2)\, j!} \left(\frac{\kappa^2 \gamma}{2\sigma_k^2 C_{1k}}\right)^{1+j} {}_1F_1\left(1+j, 2+j, \frac{-\kappa^2 \gamma}{2\sigma_k^2 C_{1k}}\right). \quad (13)$$

Proof: Please refer to Section B-A in Appendix B. ∎

Proposition 2. *When the transmit power of UAV is high, the CDF of γ_k can be approximated as* (14), *shown at the bottom of this page. Note that when m_{sk} is not an integer, j_s is an integer satisfying the condition $j_s + 1 < m_{sk} < j_s + 2$, and $\Xi\left(j\right) \triangleq \Gamma\left(m_{sk} - 1 - j\right) K_k^j \alpha_{kj}$ for all j. When m_{sk} is an integer, we set $j_s = m_{sk} - 1$, $\Xi\left(j_s\right) \triangleq K_k^{j_s} \alpha_{kj_s}$, and $\Xi\left(j\right) \triangleq \Gamma\left(m_{sk} - 1 - j\right) K_k^j \alpha_{kj}$ for $j \neq j_s$.*

Proof: Please refer to Section B-B in Appendix B. ∎

Proposition 3. *When the transmit power of UAV is high and the interference from the jamming signal is low, the CDF of γ_k can be approximated as*

$$F_{\gamma_k}^{\mathrm{HTLJ}}(\gamma) = \frac{m_k^{m_k}}{\Gamma\left(m_k\right)} \left(\frac{m_{fk}\kappa^2}{m_{fk}\kappa^2 - \Omega_k}\right)^{m_{fk}}$$
$$\times \sum_{j=0}^{M} \frac{K_k^j \alpha_{kj}}{\Gamma\left(j+1\right)\left(1+j\right)!} \left(\frac{\kappa^2 \gamma}{2\sigma_k^2 C_{1k}}\right)^{1+j}. \quad (15)$$

Proof: Please refer to Section B-C in Appendix B . ∎

With the help of (13) and (15), the derived performance metrics can be simplified. For example, the outage probability (OP) is defined as the probability that the received SNR falls below a given outage threshold γ_{th}, which means that $P_{\mathrm{out}} = \mathbb{P}\left(\gamma < \gamma_{\mathrm{th}}\right) = F_\gamma\left(\gamma_{\mathrm{th}}\right)$. The OP of the jammer-aided UAV communication system can be directly evaluated by using (11). When the interference from the jamming signal is small or the transmit power is large or both conditions are satisfied, we can use (13), (14), and (15) to obtain the corre-

$$f_{\gamma_k}(\gamma) = \frac{m_k^{m_k} \Gamma^{-1}(m_k)}{\gamma \Gamma(m_{fk}) \Gamma(m_{sk})} \left(\frac{m_{fk}\kappa^2}{\Omega_k}\right)^{m_{fk}} \sum_{j=0}^{M} \frac{K_k^j \alpha_{kj}}{\Gamma\left(j+1\right) j!} H_{1,0:0,2:1,2}^{0,0:2,0:2,1}\left(\begin{array}{c} \frac{\gamma\kappa^2}{2C_{1k}\sigma_k^2} \\ \frac{\Omega_k}{m_{fk}\kappa^2 - \Omega_k} \end{array} \middle| \begin{array}{c} (m_{fk}+m_{sk};1,1): - :(1,1) \\ - :(1+j,1)\,(m_{sk},1):(m_{fk},1)(m_{sk}+m_{fk},1) \end{array}\right) \quad (10)$$

$$F_{\gamma_k}(\gamma) = \frac{m_k^{m_k} \Gamma^{-1}(m_k)}{\Gamma(m_{fk}) \Gamma(m_{sk})} \left(\frac{m_{fk}\kappa^2}{\Omega_k}\right)^{m_{fk}} \sum_{j=0}^{M} \frac{K_k^j \alpha_{kj}}{\Gamma(j+1)\, j!} H_{1,0:0,3:1,2}^{0,0:2,1:2,1}\left(\begin{array}{c} \frac{\gamma\kappa^2}{2C_{1k}\sigma_k^2} \\ \frac{\Omega_k}{m_{fk}\kappa^2 - \Omega_k} \end{array} \middle| \begin{array}{c} (m_{fk}+m_{sk};1,1):(1,1):(1,1) \\ - :(1+j,1)(m_{sk},1)(0,1):(m_{fk},1)(m_{sk}+m_{fk},1) \end{array}\right) \quad (11)$$

sponding approximate OP expressions, respectively. Figure 2 depicts the OP performance versus the transmit power. We can observe that a good agreement exists between the analytical (*red lines*) and Monte-Carlo simulation results (*triangles*), which validates the proposed analytical expressions. In the high-transmit power regime, the approximate values obtained by (14) and (15) (*blue lines and black squares, respectively*), match well the exact ones obtained by (11). Furthermore, when the jamming power is relatively low, i.e., $P_{jk} = 10$ dBW, the calculation results of (13) (*blue circles*) are always close to the results of (11) under any transmit power.

B. Covert Performance Metrics

Then we analyze the detection behavior of warden. The warden has a binary choice between the null hypothesis, $\mathcal{H}_0$, that UAV is silent, and the alternate hypothesis, $\mathcal{H}_1$, that UAV is transmitting. Moreover, the warden can perform statistical hypothesis testing based on the received average power which includes the noise power and jamming power in $\mathcal{H}_0$ and additionally includes the received signal power in $\mathcal{H}_1$. The received signals at the warden's k_{th} antenna can be expressed as

$$y_{wk} = \begin{cases} \kappa^2 + D_{jw}^{-\alpha_{jw}} P_{jk} h_{jw}^2, & \mathcal{H}_0, \\ D_{aw}^{-\alpha_{aw}} P_{ak} h_{aw}^2 + \kappa^2 + D_{jw}^{-\alpha_{jw}} P_{jk} h_{jw}^2, & \mathcal{H}_1. \end{cases} \quad (16)$$

Let $\mathcal{D}_1$ and $\mathcal{D}_0$ represent the warden's decisions in favor of $\mathcal{H}_1$ and $\mathcal{H}_0$, respectively. The warden's decisions are based on a threshold-based rule, which is commonly adopted [8], [39], [40] and advocates $\mathcal{D}_1$ and $\mathcal{D}_0$ when the received power is larger and not larger than a predefined threshold, respectively. We can observe that erroneous decision occurs in two cases: Warden sides with $\mathcal{D}_1$ when the $\mathcal{H}_0$ is true, which is called *false alarm*, and warden sides with $\mathcal{D}_0$ when the $\mathcal{H}_1$ is true, which is called *missed detection*. The error probability is defined as the likelihood of the warden making an incorrect decision. Note that the covertness of communication is guaranteed if the warden's detection error for each user is always larger than a threshold, ξ_{th}, which is arbitrarily close to 1. Under such conditions, the communication rate is regarded as the covert rate. We use the detection error probability and covert rate to assess the system's performance in the following.

1) Detection Error Probability: The performance of warden's hypothesis test can be measured by the detection error probability, which is defined as

$$\xi_k = \mathbb{P}_{FA} + \mathbb{P}_{MD} = \Pr\left(\kappa^2 + D_{jw}^{-\alpha_{jw}} P_{jk} h_{jw}^2 > \varepsilon_k\right)$$
$$+ \Pr\left(D_{aw}^{-\alpha_{aw}} P_{ak} h_{aw}^2 + \kappa^2 + D_{jw}^{-\alpha_{jw}} P_{jk} h_{jw}^2 < \varepsilon_k\right), \quad (17)$$

where $\mathbb{P}_{FA} = \mathbb{P}(\mathcal{D}_1|\mathcal{H}_0)$ denotes the false alarm probability, and $\mathbb{P}_{MD} = \mathbb{P}(\mathcal{D}_0|\mathcal{H}_1)$ denotes the miss detection probability.

We assume that the warden can set different detection thresholds for different users to minimize the corresponding

detection error probability. Let ε_k denote the detection threshold for user U_k. The detection error probability can be obtained in Theorem 1.

Theorem 1. *The detection error probability is derived as* (18), *shown at the bottom of this page, where* $C_{1w} \triangleq D_{aw}^{-\alpha_{aw}} P_{ak}$, $C_{2w} \triangleq D_{jw}^{-\alpha_{jw}} P_{jk}$, *and* $\Omega_w \triangleq (m_{sw}-1)\bar{z}_w C_{2w}$.

Proof: Please refer to Appendix C. ∎

From (18), we can observe that the UAV and jammer can improve the covertness of communication by jointly adjusting P_{ak} and P_{jk} assigned to user U_k. However, the warden can obtain the theoretical minimum error probability by adjusting ε_k. To demonstrate the robustness of the optimal allocation algorithm, the worst-case scenario is considered where the warden can obtain the perfect CSI needed to optimize its detection threshold [41]. The warden's algorithm for optimizing the threshold is introduced in Section IV-A. If our power allocation algorithm can still guarantee that the detection error probability is arbitrarily close to 1 under the worst-case scenario, covert communication is successfully achieved.

Remark 2. *Due to channel estimation errors in practical systems, the warden may have imperfect CSI of the users. In particular, the warden has an estimated version of the channels. According to the worst-case method, channel mismatches occur in the bound set, where the upper bounds are known constants [42], i.e., e_{aw} and e_{jw} are the estimation errors of the UAV-warden and jammer-warden links, respectively. Thus, the DEP achieved by the warden based on imperfect CSI can be expressed as $\xi_k' = \Pr\left(D_{aw}^{\alpha_{aw}} P_{ak}(h_{aw}+e_{aw})^2 + \kappa^2 + D_{jw}^{\alpha_{jw}} P_{jk}(h_{jw}+e_{jw})^2 < \varepsilon_k\right) + \Pr\left(\kappa^2 + D_{jw}^{\alpha_{jw}} P_{jk}(h_{jw}+e_{jw})^2 > \varepsilon_k\right)$. Because the PDF and CDF of both h_{aw} and h_{jw} are known, we can obtain the statistical expressions of $(h_{aw}+e_{aw})$ and $(h_{jw}+e_{jw})$ easily. Then, by following the same derivation methods in Appendix C, the closed-form expression of DEP with imperfect CSI can be obtained. Note that if the warden uses the expression of DEP with imperfect CSI to determine the threshold, the warden will inaccurately select the detection threshold that does not achieve the minimal DEP, as shown in Fig. 6.*

Remark 3. *If we consider that the jammer uses multiple antennas, i.e., L_J antennas, to assist one user, we can design the jamming signal beamforming vector to achieve better covertness. Let $\mathbf{h_{jw}} = [h_{jw,1}, h_{jw,2}, \ldots, h_{jw,L_J}]$ denote the MISO channel fading vector between the jammer and the warden, and $\mathbf{v_k} = [v_{k,1}, v_{k,2}, \ldots, v_{k,L_J}]$ denote the jamming signal vector, where $\|\mathbf{v_k}\| \leq 1$. Then, the received jamming signal can*

$$F_{\gamma_k}^{\text{HT}}(\gamma) = \frac{m_k^{m_k}}{m_{sk}\Gamma(m_k)B(m_{sk}, m_{fk})} \left(\frac{\Omega_k}{m_{fk}} \frac{1}{2\sigma_k^2} \frac{\gamma}{C_{1k}}\right)^{m_{sk}} \sum_{j=j_s+1}^{M} \frac{\Gamma(1+j-m_{sk})K_k{}^j \alpha_{kj}}{\Gamma(j+1)j!} + \frac{m_k^{m_k}}{\Gamma(m_k)\Gamma(m_{sk})} \left(\frac{m_{fk}\kappa^2}{\Omega_k}\right)^{m_{fk}}$$
$$\times \sum_{j=0}^{j_s} \frac{\Xi(j)}{B(m_{fk}+m_{sk}-j-1, j+1)(j+1)!} \left(\frac{\kappa^2\gamma}{2\sigma_k^2 C_{1k}}\right)^{j+1} {}_2F_1\left(m_{fk}, m_{sk}+m_{fk}; m_{fk}+m_{sk}-j-1; \frac{\Omega_k-m_{fk}\kappa^2}{\Omega_k}\right) \quad (14)$$
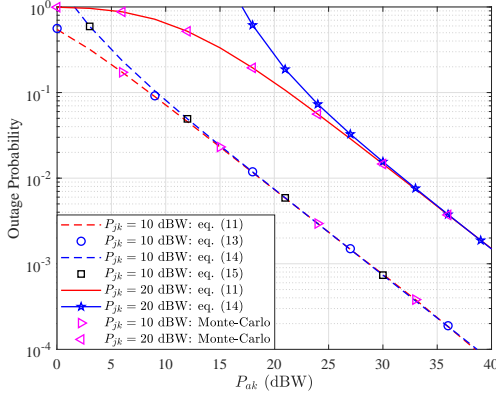
Fig. 2. The outage probability versus the transmit power, with $m_k = 2$, $K_k = 2$, $2\sigma_k^2(1 + K_k) = 15$ dB, $\Delta_k = 0.7$, $\kappa^2 = 1$ dB, $m_{fk} = 3$, $m_{sk} = 3$, $\bar{z}_k = 1$, $\gamma_{th} = 1$, $D_{jk} = 10$ m, $D_{ak} = 5$ m, $\alpha_{jk} = 3$, $\alpha_{ak} = 2$, and different values of jamming power.

be expressed as $y_{jw} = \sqrt{D_{jw}^{-\alpha_{jw}}} \mathbf{h_{jw}v_k}^T$. Using the maximum ratio transmitting [43], [44], we can define $\mathbf{v_k}$ as $\mathbf{v_k} = \mathbf{h_{jw}}/\|\mathbf{h_{jw}}\|$, and the corresponding DEP is re-written as $\xi_k^{(MRT)}$

$$= \Pr\left(D_{aw}^{\alpha_{aw}}P_{ak}(h_{aw}+e_{aw})^2 + \kappa^2 + P_{jk}D_{jw}^{\alpha_{jw}}\left(\sum_{\ell=1}^{L_J} h_{jw,\ell}\right)^2 < \varepsilon_k\right) +$$

$$\Pr\left(\kappa^2 + P_{jk}D_{jw}^{\alpha_{jw}}\left(\sum_{\ell=1}^{L_J} h_{jw,\ell}\right)^2 > \varepsilon_k\right).$$ Because $h_{jw,\ell}$ is the Fisher-Snedecor $\mathcal{F}$ RV, the distribution of the sum of L_J $\mathcal{F}$ RVs, i.e., $\sum_{\ell=1}^{L_J} h_{jw,\ell}$, can be approximated by the single Fisher-Snedecor $\mathcal{F}$ fading distribution [45]. Thus, we can analyze the DEP following similar methods in Theorem 1.

2) Covert Communication Rate: Using the PDF and CDF expressions of γ_k in Lemma 1, we can obtain the covert rate of the user U_k.

Theorem 2. *In our considered system, the covert rate of the k-th user is given by* (19), *shown at the bottom of the next page.*

Proof: Please refer to Appendix D. ∎

While ensuring that the communication is covert, every user wants to communicate at a rate as high as possible. From (19), we can observe that, except for the unchangeable channel coefficients, the maximum covert rate for user U_k can be achieved by adjusting P_{ak} and P_{jk}. To allocate the limited resources fairly to multiple users, we next formulate the problem with the help of game theory by regarding users as players in a bargaining game.

IV. PROBLEM FORMULATION

The user's QoS requirements consist of two categories, which are the covertness of communication and the transmission performance. To achieve covert communication, each user asks for an adequate amount of jammer power. Additionally, each user wants the UAV to assign an adequate amount of transmit power to improve the covert rate. However, there are two key challenges:

- If too much transmit power is provided to a single user, the communication's covertness may be compromised, as warden can detect the transmission more accurately. Furthermore, because the jamming and the data signals are in the same frequency band, too high jamming power will reduce the covert rate. As a result, we have to optimize the allocation of transmit and jamming power.
- There are K users being served at the same time, but both the transmit power of the UAV and jamming power of the jammer are restricted. Limited resources lead to gaming among users. Thus, we may use the bargaining game theory to solve the power allocation problem. The users can be viewed as the players in the game.

To tackle the aforementioned two key challenges, we represent the optimization problem as a bargaining game to maximize the user's covert rate with limited transmit and jamming power, while ensuring the covertness. To demonstrate the robustness, the game is modeled under the warden's optimal detection threshold, which represent the worst-case scenario for the users. In the following, we introduce the method for the warden to obtain the optimal threshold, and then propose the bargaining game model.

A. Optimal Detection Threshold at Warden

1) Convergence Analysis: From (18), we can see that the detection threshold, ε_k, transmit and jamming powers exist in both Gauss hypergeometric function and multivariate Fox's H-function, which means that it is difficult to analyze whether (18) is convex directly. Therefore, we first study the following integral equation.

Lemma 2. *The* $I_L \triangleq \int_{T_1}^{T_2} t^A(B - t)^C e^{-Dt}dt$ *with different cases of* T_1 *and* T_2 *can be derived as* (20), *shown at the bottom of the next page, where* U *is the tricomi confluent hypergeometric function* [46].

Proof: Please refer to Appendix E. ∎

To the best of our knowledge, an exact solution of I_L cannot be found in any function books, e.g., [26]–[28]. For the third case, i.e., when $(T_1 = 0, T_2 = \infty)$, due to the complexity of the tricomi confluent hypergeometric function, it may be difficult to be used for convergent analysis. Thus, we derive two kinds of approximate results. As shown in Fig. 3, the approximation expressions that we obtain are highly accurate. For the first two cases, the approximate expressions can be obtained following the similar methods in Proposition 2.

Because that the exponential function is common in many channel fading models [22], [23], [34], Lemma 2 is useful in the performance analysis of wireless communications systems. Using Lemma 2, we can analyze (18) to prove its convexity in the following theorem.

Theorem 3. *Under a given allocation scheme of transmit and jamming power, the detection error probability is convex with respect to the detection threshold,* ε_k.

Proof: Please refer to Appendix F. ∎

Therefore, the optimal detection threshold, ε_k^{opt}, can be derived by solving $\frac{\partial \xi_k}{\partial \varepsilon_k} = 0$. However, in many cases, the

warden cannot obtain the perfect channel state information. Thus, in the following, we propose a PSO-based optimization algorithm, where the warden only needs to know the values of its detection error probability.

2) Particle Swarm Optimization (PSO) Algorithm: In the PSO algorithm, n particles travel in an L-dimensional search space to optimize the fitness function [47]. In our case, L is equal to 1. First, the particles are dispersed randomly in the search space, where each particle's position indicates a possible solution to the fitness function. Then, in every iteration, each particle evaluates the fitness and travels to a new place based on the history of the particle's best prior location and the global best position. The velocity v_i and position x_i of the i_{th} particle are updated using the following equations

$$v_i(k+1) = \omega v_i(k) + c_1 R_1(p_i(k) - x_i(k)) + c_2 R_2(p_g(k) - x_i(k)),$$
(21a)

$$x_i(k+1) = x_i(k) + v_i(k+1),$$
(21b)

for $i = 1, 2, \ldots, m$, where ω is the inertia weight, c_1 and c_2 are acceleration constants, both R_1 and R_2 are uniformly distributed in $[0, 1]$, p_i is the best previous position, and p_g is the best global position in the swarm.

To minimize ξ_k by adjusting ε_k, the warden can initialize n particles to search for the optimal detection threshold, ε_k^{opt}. The detailed PSO algorithm is given in Algorithm 1. Because we have proven that ξ_k is convex with respect to ε_k, Algorithm 1 can converge quickly. The total running time of Algorithm 1 can be expressed as $n\text{M}_{\text{PSO}}T_T$, where T_T is the time required by per particle in one iteration [48].

B. Game Theoretic Problem Formulation

Several multi-user communication scenarios have been studied with game-theoretic bargaining solutions, e.g., OFDMA channel allocation [49], bandwidth allocation for multimedia [50], and rate control for video coding [51]. In cooperative games, players, i.e., K users, aim to reach an agreement that is efficient and fair given the five axioms of PAR, IR, INV, IIA and SYM [21]. Each user U_k has its own utility function and a minimum desired utility, called the disagreement point. The disagreement point is the minimum utility that each user expects. In our case, the resource is the transmitting and jamming power, and the utility function of user U_k can be defined as $U_k(P_{ak}, P_{jk})$. Let $S = \{U_1, \ldots, U_K\}$ denote a joint utility set that is nonempty, convex, closed, and bounded, and $D = \{U_1^{th}, \ldots, U_K^{th}\}$

Algorithm 1 The particle swarm optimization for finding the optimal detection threshold for user U_k.

Input: Input the size of swarm: n, maximum velocity: $v_{\max}$, inertia weight: ω, acceleration constants: c_1 and c_2, iteration numbers: M$_{\text{PSO}}$

Output: The optimal detection threshold: ε_k^{opt}.

1: *Initialize the velocities and positions of n particles, where the position means different ε_k for user k*
2: **for** Every particle in swarm **do**
3:    *Obtain ξ_k with the help of* (18)
4: Update personal and global best positions, and corresponding values
5: **while** $k < \text{M}_{\text{PSO}}$ **do**
6:    **for** Every particle **do**
7:       *Obtain corresponding ξ_k with the help of* (18)
8:       **if** Current position is personal best position **then**
9:          Update its personal best position
10:    *Update global best positions (a set of detection thresholds for K users), and corresponding fitness function values (detection error probability)*
11:    **for** Every particle **do**
12:       Update v with the help of (21a)
13:       **if** $v > v_{\max}$ **then**
14:          $v \leftarrow v_{\max}$
15:       Update x with the help of (21b)
16:       **if** $x \leq \kappa^2$ **then**
17:          $x = \kappa^2$
18: $\varepsilon_k^{opt} = \varepsilon_k$
19: **return** The global best position: ε_k^{opt}

---

denote the disagreement point set. The pair (S, D) defines the bargaining problem.

As an efficient resource allocation strategy, the NBS has been extensively deployed as a fair solution for the NBG [21].

$$\xi_k = 1 - \frac{m_{fw}{}^{m_{fw}-1}(\varepsilon_k - \kappa^2)^{m_{fw}}}{C_{2w}{}^{m_{fw}} B(m_{fw}, m_{sw})(m_{sw}-1)^{m_{fw}} \bar{z}_w{}^{m_{fw}}} \, _2F_1\left(m_{fw}, m_{fw}+m_{sw}, m_{fw}+1; -\frac{m_{fw}(\varepsilon_k-\kappa^2)}{\Omega_w}\right)$$
$$+ \frac{m_w{}^{m_w}}{\Gamma(m_{fw})\Gamma(m_{sw})\Gamma(m_w)} \sum_{j=0}^{\infty} \frac{K_w{}^j \alpha_{wj}}{j!\,\Gamma(j+1)} H_{1,0:1,3:1,1}^{0,0:3,0:1,1}\left(\left.\begin{array}{c} \frac{\Omega_w}{m_{fw}(\varepsilon_{th}-\kappa^2)} \\ \frac{2C_{1w}\sigma_w^2}{\varepsilon_{th}-\kappa^2} \end{array}\right| \begin{array}{c} (1;1,1):(1-m_{fw},1)(1,1):(-j,1) \\ -:(0,1)(m_{sw},1)(1,1):(0,1) \end{array}\right) \quad (18)$$

$$R_k = \frac{-m_k{}^{m_k}\Gamma^{-1}(m_k)}{\ln 2\,\Gamma(m_{fk})\Gamma(m_{sk})}\left(\frac{m_{fk}\kappa^2}{\Omega_k}\right)^{m_{fk}} \sum_{j=0}^{\infty} \frac{K_k{}^j \alpha_{kj}}{\Gamma(j+1)\,j!} H_{1,0:1,3:1,2}^{0,0:3,1:2,1}\left(\left.\begin{array}{c} \frac{\kappa^2}{2C_{1k}\sigma_k^2} \\ \frac{\Omega_k}{m_{fk}\kappa^2-\Omega_k} \end{array}\right| \begin{array}{c} (m_{fk}+m_{sk};1,1):(1,1):(1,1) \\ -:(1+j,1)(m_{sk},1)(0,1):(m_{fk},1)(m_{sk}+m_{fk},1) \end{array}\right) \quad (19)$$

With the help of NBS, our problem can be formulated as

$$\max_{\{P_{jk}, P_{ak}\}} \quad \prod_{k=1}^{K} \left(R_k - R_k^{\text{th}} \right) \tag{22a}$$

$$\text{s.t.} \quad \sum_{k=1}^{K} P_{jk} \leqslant P_J, \tag{22b}$$

$$\sum_{k=1}^{K} P_{ak} \leqslant P_T, \tag{22c}$$

$$\xi_k \geqslant \xi_k^{\text{th}}, \forall k, \tag{22d}$$

where R_k can be calculated as in (19), ξ_k^{th} is a constant which is close to 1, and ξ_k can be obtained by (18) under the optimal detection threshold.

Note that our problem and solution are equivalent to standard Nash bargaining problem, and hence these five axioms that mentioned before are achievable intrinsically. However, the computational complexity required to find an NBS significantly increases as the number of users increases, which makes it difficult to obtain optimal allocation solutions given both P_T and P_J simultaneously. To solve the aforementioned issues, we propose the following two efficient algorithms and analyze their converge.

V. Joint Jamming and Transmitting Power Allocation Algorithm

In this section, we propose two algorithms, i.e., PPA and JTPA algorithms, for jammer-aided multi-antenna UAV covert communication networks. In the PPA algorithms, we let n particles travel in a $2K$-dimensional convex search space. In the JTPA algorithm, we first optimize the jamming power allocation under the fixed transmit power allocation in Stage 1. Then, in Stage 2, we aim to determine the best transmit power allocation based on the results of Stage 1. The overall algorithm stops until the convergence is achieved.

A. Convergence Analysis

According to the definition of the covert rate as (D-1) in Appendix D, the cover rate increases monotonically with the increase of transmit power and decreases monotonically with the increase of jamming power. In the following, we first prove that the constraint set is a convex feasible set. Note that the

power constraints, (22b) and (22c), are convex with respect to P_{jk} and P_{ak}, respectively. For (22d), the Hessian matrix can be expressed as

$$\nabla^2 \xi_k = \left| \begin{array}{cc} \frac{\partial^2 \xi_k}{\partial C_{1w}^2} & \frac{\partial^2 \xi_k}{\partial C_{1w} \partial C_{2w}} \\ \frac{\partial^2 \xi_k}{\partial C_{2w} \partial C_{1w}} & \frac{\partial^2 \xi_k}{\partial C_{2w}^2} \end{array} \right|. \tag{23}$$

Theorem 4. *The Hessian matrix of ξ_k is semi-negative definite.*

Proof: Please refer to Appendix G. ■

Therefore, we conclude that the constraint set is convex. However, from the expression of fitness function (19), we can observe that the parameters P_{jk} and P_{ak} exist in one Fox's H-function. Thus, it is difficult, if not impossible, to derive the analytical expression of optimal P_{jk} and P_{ak}. Fortunately, by regarding (18) as the fitness function, many kinds of search algorithms, i.e., PSO, can be used to obtain the maximum ξ_k and corresponding ε_k because the search space is convex. Moreover, alternating optimization could also be used to trade off between the system performance and computational complexity.

B. PSO-based Power Allocation Algorithm

Because $\mathbb{P}_{FA}$ is not related to P_{ak}, and $\mathbb{P}_{MD}$ increases as P_{ak} increases, (22d) limits the ceiling of P_{ak}. For given P_{ak}, ξ_k is concave with the respect to P_{jk} (see Appendix G). Thus, (22b)-(22d) actually limit the ranges of P_{ak} and P_{jk}, which can be regarded as the boundary to PSO's search space. In the following, the PSO algorithm used for searching the maximum of objective function is proposed.

To find the maximum $\prod_{k=1}^{K} \left(R_k - R_k^{\text{th}} \right)$, we propose a PSO algorithm, denoted by Algorithm 2, under the particles' location limitation given in (22b)-(22d)[1]. Different from Algorithm 1, the output now is the optimal transmit and jamming power allocation, $\{P_{j1}^{opt}, \ldots, P_{jK}^{opt}\}$ and $\{P_{a1}^{opt}, \ldots, P_{aK}^{opt}\}$, the fitness function is $\prod_{k=1}^{K} \left(R_k - R_k^{\text{th}} \right)$, and the dimension of searching space is $2K$ because the $2K$ coordinates of each particle

---

[1]To save the space, we discuss the differences between Algorithm 2 and Algorithm 1 here, instead of giving the specific Algorithm 2.

$$\int_{T_1}^{T_2} t^A (B-t)^C e^{-Dt} dt =$$

$$\begin{cases}
\text{Cases} & \text{Results} & \text{Conditions} \\
\begin{array}{c} T_1=0, \\ T_2=T \end{array} & I_{L_1} = \frac{B^C T^{1+A}}{\Gamma(-C)} H_{1,1:0,1;1,1}^{0,1:1,0;1,1}\left(\left. \begin{array}{c} DT \\ -B^{-1}T \end{array} \right| \begin{array}{c} (-A;1,1):-:(1+C,1) \\ (-1-A;1,1):(0,1):(0,1) \end{array} \right) & \begin{array}{c} \{\text{Re}\left\{\frac{B}{T}\right\} > 1 \| \text{Re}\left\{\frac{B}{T}\right\} \leq 0 \| \frac{B}{T} \notin \text{Re}\} \\ \& \text{Re}\{D\} > 0 \& C \neq 0, -1, -2, \ldots \end{array} \\
\begin{array}{c} T_1=T, \\ T_2=\infty \end{array} & \begin{array}{c} I_{L_2} = (-1)^C (T_1)^{1+A+C} \\ \times H_{2,1:2,0;0,1}^{0,2:0,1;1,0}\left(\left. \begin{array}{c} (DT_1)^{-1} \\ -BT^{-1} \end{array} \right| \begin{array}{c} (2+A+C;1,1)(-A,-1,1):(1,1)(1+A,1):- \\ (1+A+C;1,1):-:(0,1) \end{array} \right) \end{array} & \begin{array}{c} \text{Re}\{B\} > 0 \& \text{Re}\{D\} > 0 \\ \& \text{Re}\{T\} > 0 \& \text{Im}\{T\} = 0 \end{array} \\
\begin{array}{c} T_1=0, \\ T_2=\infty \end{array} & \begin{array}{c} I_{L_3} = \Gamma(1+A) B^C (-B)^{1+A} U(1+A, 2+A+C, -BD) \\ \approx \Gamma(1+A) B^C D^{-A-1}, \text{(when } B \text{ or } D \text{ is large)} \\ \approx \frac{\Gamma(-1-A-C)}{\Gamma(-C)} + \frac{\Gamma(1+A+C)}{\Gamma(1+A)(-BD)^{1+A+C}}, \text{(when } B \text{ or } D \text{ is small)} \end{array} & \begin{array}{c} \text{Re}\{A\} > -1 \& \text{Re}\{B\} > 0 \\ \& \text{Re}\{D\} > 0 \end{array} \\
\begin{array}{c} T_1=0, \\ T_2=B \end{array} & I_{L_4} = \frac{B^{1+A+C}\Gamma(1+A)\Gamma(1+C)}{\Gamma(2+A+C)} {}_2F_1(1+A, 2+A+C, -BD) & \begin{array}{c} \text{Re}\{A\} > -1 \& \text{Re}\{C\} > -1 \\ \& \text{Re}\{B\} > 0 \& \text{Im}\{B\} = 0 \end{array}
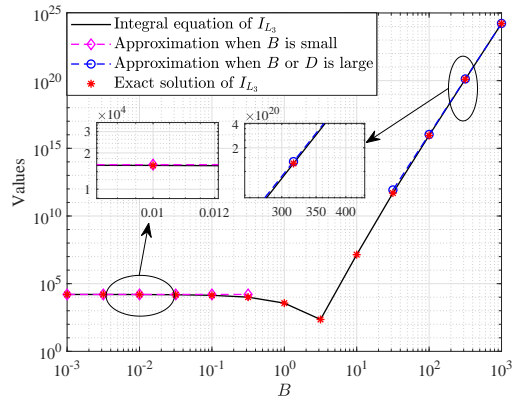\end{cases} \tag{20}$$

Fig. 3. Equation real-part values on the left and right-hand sides of I_{L_3} versus B, with $A = 3.2$, $C = 8.2$, $D = 2$.

Algorithm 2: Particle Swarm Optimization-Based Power Allocation Algorithm
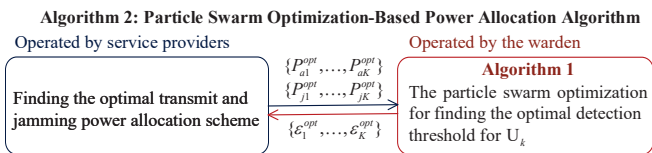

Fig. 4. The relationship of service providers' (i.e., UAV and jammer) PPA algorithm and the warden's detection threshold optimization algorithms: The transmit and jamming power will affect the optimal detection threshold, while the changing of detection threshold will change the optimal power allocation scheme simultaneously.

represent one possible transmit and jamming power allocation scheme. Note that when the UAV and jammer are adjusting the joint power allocation schemes, the warden is optimizing its detection threshold based on the current transmit and jamming power. Furthermore, the detection threshold will also affect the Algorithm 2, as shown in Fig. 4. The total running time of Algorithm 2 is $T_P = 2nKT_T\mathrm{M_{PSO}}$, where T_T denotes the time required by per particle in one iteration, $\mathrm{M_{PSO}}$ is the iteration number, and n denotes the size of swarm.

C. Joint Two-Stage Power Allocation Algorithm

To reduce the computational complexity, we further propose an efficient two-stage power allocation algorithm based on the alternating optimization of the transmit and jamming power in an iterative manner. Note that maximizing $\prod_{k=1}^{K} \left(R_k - R_k^{\mathrm{th}} \right)$ equals to maximize $\sum_{k=1}^{K} \ln \left(R_k - R_k^{\mathrm{th}} \right)$. Moreover, if $\left(R_k - R_k^{\mathrm{th}} \right)$ is concave, $\ln \left(R_k - R_k^{\mathrm{th}} \right)$ is also concave because $\left(\ln \left(F_k \right) \right)'' = \frac{F_k{}'' F_k - \left(F_k{}' \right)^2}{F_k{}^2}$, where $F_k \triangleq R_k - R_k^{\mathrm{th}}$, $(\cdot)'$ denotes the first order derivative and $(\cdot)''$ denotes the second order derivative.

1) Stage 1: Optimization of Jamming Power: For any given transmit power allocation, the jamming power allocation problem can be formulated as

$$\max_{\{P_{jk}\}} \quad \sum_{k=1}^{K} \ln \left(R_k - R_k^{\mathrm{th}} \right) \tag{24a}$$

$$\text{s.t.} \quad (22\mathrm{b}), (22\mathrm{c}), (22\mathrm{d}). \tag{24b}$$

If the transmit power allocated to a user by the UAV is too high, the warden's detection error probability for that user will decrease, resulting in a failure of covert communication. Therefore, the jammer needs to allocate the appropriate amount of power to interfere the detection of the warden. Although the jamming signals will also affect the user's SINR and cause a decrease in the covert rate, the interference that it causes to the warden allows the UAV to utilize a higher transmit power for data transmission, thus ultimately increasing the cover rate after transmit power optimization compared to the absence of jamming signals [37]. Note that (24a) can be solved using swarm intelligence algorithms [52] or the method of Lagrange multipliers [53], which have been widely studied [54]–[57].

2) Stage 2: Optimization of Transmit Power: In Stage 2, we design the optimal transmit power allocation scheme under the fixed jamming power. The problem can be formulated as

$$\max_{\{P_{ak}\}} \quad \sum_{k=1}^{K} \ln \left(R_k - R_k^{\mathrm{th}} \right) \tag{25a}$$

$$\text{s.t.} \quad (22\mathrm{b}), (22\mathrm{c}), (22\mathrm{d}). \tag{25b}$$

This problem can be solved by the similar method as in Stage 1. Although an increase in transmit power may decrease the detection error probability of warden, the jamming power allocation scheme proposed in Stage 1 can help to increase the detection error probability.

3) Joint Two-Stage Power Allocation Algorithm: Based on the results presented in the previous two subsections, we propose a two-stage alternating iterative algorithm. Specifically, let $\mathbf{P_j} = \{P_{j1}, \ldots, P_{jK}\}$ and $\mathbf{P_a} = \{P_{a1}, \ldots, P_{aK}\}$. In the $(r+1)$ iteration, we use a fixed $\mathbf{P}_a^{(r)}$ to obtain $\mathbf{P}_j^{(r+1)}$ in Stage 1. Then, with the help of $\mathbf{P}_j^{(r+1)}$, $\mathbf{P}_a^{(r+1)}$ is solved in Stage 2. The overall algorithm stops iterating when the difference between the objective function values obtained in two iterations is less than a threshold. The procedure of the JTPA is summarized in Algorithm 3.

While the UAV and jammer are using Algorithm 3 for power allocation, the warden is also using Algorithm 1 for optimal detection threshold design. Since the UAV, jammer, and the warden are working simultaneously and interacting with each other, we give Fig. 5 to show the relationship of the five algorithms proposed in this paper.

VI. NUMERICAL RESULTS

In this section, simulation results are presented to verify the proposed PPA and JTPA algorithms for jammer-aided multi-antenna UAV covert communication networks. We set $K = 3$, and the locations of the three users, the jammer, the UAV, and the warden are $\mathbf{q}_1 = [0, 10, 0]^T$, $\mathbf{q}_2 = [7, 14, 0]^T$, $\mathbf{q}_3 = [5, 20, 0]^T$, $\mathbf{q}_j = [7, 24, 0]^T$, $\mathbf{q}_a = [5, 13, 20]^T$, and $\mathbf{q}_w = [5, 16, 0]^T$, respectively. The coefficients of path loss model are $\alpha_{a1} = 1$, $\alpha_{a2} = 1.2$, $\alpha_{a3} = 1.3$, $\alpha_{aw} = 1.2$, $\alpha_{j1} = 1.7$, $\alpha_{j2} = 1.6$, $\alpha_{j3} = 1.8$, $\alpha_{jw} = 1.7$. The AWGN power is $\kappa^2 = 3$ dB. For parameters of Fisher-Snedecor $\mathcal{F}$ fading model, we set $m_{f1} = 2$, $m_{f2} = 3$, $m_{f3} = 5$, $m_{fw} = 3$, $m_{s1} = 4$, $m_{s2} = 4$, $m_{s3} = 5$, $m_{sw} = 4$, $\bar{z}_1 = -10$ dB, $\bar{z}_2 = -12$ dB, $\bar{z}_3 = -13$ dB, and $\bar{z}_w = -11$ dB. For parameters of FTR

Algorithm 3 Joint two-stage transmit and jamming power allocation algorithm.

Input: Input the size of swarm: n, dimension of searching space: K, maximum velocity: $v_{\max}$, inertia weight: ω, acceleration constants: c_1 and c_2, iteration numbers: M_{PSO}

Output: The transmit and jamming power allocation schemes: $\{P_{j1}^{opt}, \ldots, P_{jK}^{opt}\}$ and $\{P_{a1}^{opt}, \ldots, P_{aK}^{opt}\}$

1: Initialize $\mathbf{P}_a^{(0)}$ and $\mathbf{P}_j^{(0)}$, calculate the objective function as $\sum_{k=1}^{K} \ln\left(R_k - R_k^{\mathrm{th}}\right)^{(0)}$, set the iteration number: $r = 0$, set the threshold: ρ.

2: **repeat**

3:     Stage 1: For fixed $\mathbf{P}_a^{(r)}$, solve (24) to obtain $\mathbf{P}_j^{(r+1)}$.

4:     Stage 2: For fixed $\mathbf{P}_j^{(r+1)}$, solve (25) to obtain $\mathbf{P}_a^{(r+1)}$.

5:     Denote the objective function as $\sum_{k=1}^{K}\ln\left(R_k - R_k^{\mathrm{th}}\right)^{(r+1)}$.

6:     $r = r + 1$.

7: **until** $\left|\sum_{k=1}^{K} \ln\left(R_k - R_k^{\mathrm{th}}\right)^{(r)} - \sum_{k=1}^{K} \ln\left(R_k - R_k^{\mathrm{th}}\right)^{(r-1)}\right| < \rho$

8: $\{P_{j1}^{opt}, \ldots, P_{jK}^{opt}\} = \{P_{j1}, \ldots, P_{jK}\}$ and $\{P_{a1}^{opt}, \ldots, P_{aK}^{opt}\} = \{P_{a1}, \ldots, P_{aK}\}$.

9: **return** The global best position: $\{P_{j1}^{opt}, \ldots, P_{jK}^{opt}\}$ and $\{P_{a1}^{opt}, \ldots, P_{aK}^{opt}\}$.
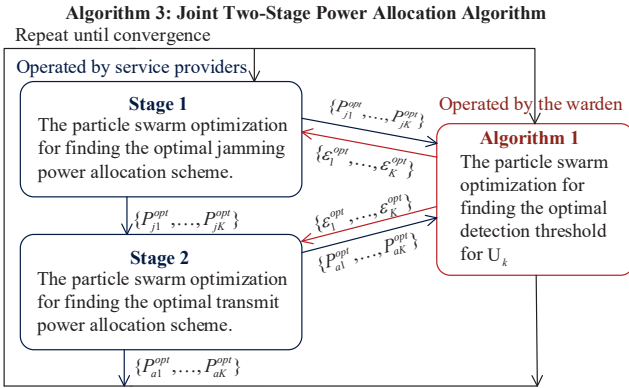

Fig. 5. The relationship of service providers' (i.e., UAV and jammer) JTPA algorithm and the warden's detection threshold optimization algorithms: In Stage 1, the service providers adjust the jamming power, and the warden will obtain a set of corresponding detection thresholds. In Stage 2, the service provider will obtain the optimal transmit power based on the current thresholds. Then we go back to Stage 1 again until the convergence is achieved.

fading model, we set $m_1 = 4$, $m_2 = 3$, $m_3 = 5$, $m_w = 4$, $K_1 = 4$, $K_2 = 5$, $K_3 = 5$, $K_w = 3$, $\Delta_1 = 0.5$, $\Delta_2 = 0.5$, $\Delta_3 = 0.4$, $\Delta_w = 0.4$, $2\sigma_1^2(1+K_1) = -10$ dB, $2\sigma_2^2(1+K_2) = -15$ dB, $2\sigma_3^2(1+K_3) = -11$ dB, and $2\sigma_w^2(1+K_w) = -10$ dB.

Figure 6 shows the detection error probability, ξ_k ($k = 1, 2, 3$), versus the detection threshold with or without our proposed JTPA algorithm, with $P_T = 20$ dBW, $P_J = 20$ dBW, and $\xi_k^{\mathrm{th}} = 95\%$. Under the fixed total power parameters (i.e., P_T and P_J), we can observe that each curve has its optimal detection threshold which can be captured by the warden. With the help of Algorithm 1, the optimal detection threshold for each user obtained by the warden is marked with stars. Note that each link's corresponding detection error probability fails
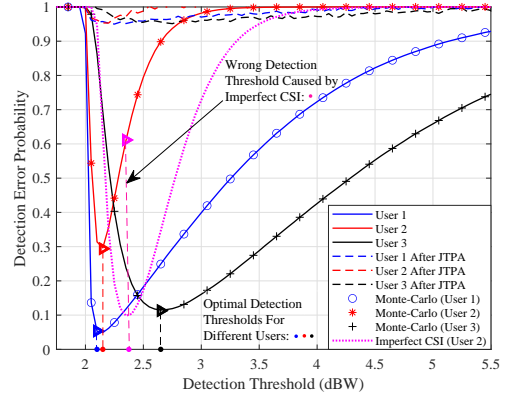

Fig. 6. The detection error probability, ξ_k ($k = 1, 2, 3$), versus the detection threshold with or without our proposed JTPA algorithm, with $P_T = 20$ dBW, $P_J = 20$ dBW, and $\xi_k^{\mathrm{th}} = 95\%$.
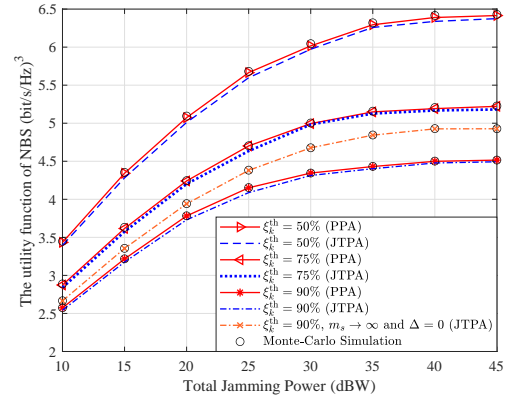

Fig. 7. The NBS's utility function versus with the jammer's available total power under the different detection error thresholds, with $P_T = 30$ dBW.

to achieve the covertness requirements. Thus, it is necessary to use our PPA or JTPA algorithms to ensure the covertness of communication. As shown by the dotted lines in Fig. 6, all users' communication can make the warden's detection error probability reach more than 95% and be turned into secure ones, even under the warden's optimal detection threshold. Specifically, the error probabilities of users U_k ($k = 1, 2, 3$) increase 1800%, 196% and 691%, respectively. These results demonstrate the effectiveness of our proposed JTPA algorithm. Furthermore, if the CSI is imperfectly estimated, the warden will choose the wrong detection threshold and fail to achieve the minimal DEP. For example, when $e_{jw} = e_{aw} = -10$ dB, the corresponding DEP is 107.9% higher than the minimal one.

Figure 7 depicts the NBS's utility function versus the jammer's available total power under the different detection error thresholds, with $P_T = 20$ dBW. More specifically, the utility function increases with the increase of the available total power of the jammer, e.g., we can observe that the utility function increases by 78% when P_J increases from 10 dBW to 30 dBW with $\xi_k^{\mathrm{th}} = 75\%$. Another interesting insight is that the utility is higher when the ξ_k^{th} is lower. For example, when ξ_k^{th} decreases from 90% to 50% with $P_J = 30$ dBW, the utility

Fig. 8. The NBS's utility function versus the total transmit power of UAV, under different sets of total transmit powers of UAV, with $\xi_k^{\text{th}} = 90\%$.

Fig. 9. The NBS's utility versus the UAV's location, with $P_T = 20$ dBW, $P_J = 20$ dBW, $\mathbf{q}_1 = [3, 15, 0]^T$, $\mathbf{q}_2 = [6, 18, 0]^T$, $\mathbf{q}_3 = [8, 12, 0]^T$, and $\xi_k^{\text{th}} = 90\%$.

function increases by 39%. The reason is that a high ξ_k^{th} means that the system has high standards for covertness. Thus, the UAV has to allocate lower transmit power to users to meet the covertness requirements, especially when the available total power of the jammer is scarce or the jammer is located in a relatively distant position. In contrast, we can deploy a higher UAV's transmit power P_T to enhance the system's utility when the jammer has sufficient power to dramatically degrade the warden's detection capability and provide a greater margin for the system's utility. For special small-scale fading cases, i.e., $m_s \to \infty$ (Fisher-Snedecor $\mathcal{F} \to$ Nakagami-m) and $\Delta = 0$ (FTR fading $\to$ Rician shadowed fading), the total utility is higher because of better channel quality. However, the utility no longer increases with the jammer's total power in the high-jamming power range, because the total jamming power at this range is sufficient for three users. Furthermore, we can observe that the utility achieved by PPA algorithm is sightly larger then that achieved by JTPA algorithm. The reason is that there is no iteration in the PPA algorithm. However, JTPA is more efficient because PPA algorithm requires $2K$ particles in the search space simultaneously.

As a supplement, Fig. 8 shows the NBS's utility function versus the total transmit power of UAV, under different sets of total transmit powers of UAV, with $\xi_k^{\text{th}} = 90\%$. Figure 8 illustrates that a higher total transmit power P_T can achieve a larger utility function of NBS. It is interesting that when the total transmit power is small, the utility functions at different total jamming powers are very close to each other. The reason is that the jamming power required to achieve a high detection error probability is low when the transmit power is low. When the total transmit power is larger, we can observe that the difference between utility functions under different total jamming power is larger. For example, when $P_T = 30$ dBW, the utility function increases 22% when P_J increases from 10 dBW to 20 dBW. Furthermore, due to the covertness requirements, we can observe that there is an upper bound of the UAV's transmit power where the utility no longer increases with its total power. The case without jammer is also shown in Fig. 8. We can observe that the utility achieved with the help of jammer is significantly larger. Combined with the result
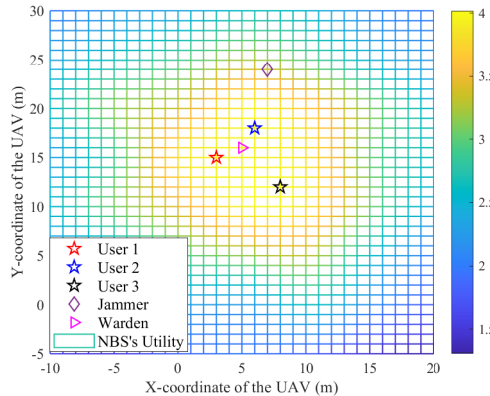
in Fig. 7, it is proved that the jammer's total power and the UAV's transmit power jointly determine the system's utility, and our proposed PPA and JTPA algorithms are effective.

To further illustrate the impact of the UAV's location on the NBS's utility, Fig. 9 plots the relationship between the horizontal plane coordinate (the height of UAV is fixed) and the NBS's utility function, with $P_T = 20$ dBW, $P_J = 20$ dBW, $\mathbf{q}_1 = [3, 15, 0]^T$, $\mathbf{q}_2 = [6, 18, 0]^T$, $\mathbf{q}_3 = [8, 12, 0]^T$ and $\xi_k^{\text{th}} = 90\%$. For each point shown in Fig. 9, the PPA and JTPA algorithms are used to maximize the covert rate, which also proves the effectiveness of our algorithms even when the UAV's position varies over a wide range. Furthermore, in Fig. 9, we can observe that the value of the utility function can be further improved by UAV's trajectory planning optimization. Within the flying range shown in Fig. 9, The utility function when the UAV is in the optimal position is 167% higher than that when the UAV is in the worst position. The detailed analysis is left for the future work.

VII. Conclusion

A jammer-aided multi-antenna UAV covert communication system is investigated. We used the Fisher-Snedecor $\mathcal{F}$ fading and FTR fading to derive the exact PDF and CDF of the SINR. Important covert performance metrics including detection error probability and covert rate were derived. With the help of the obtained performance metrics, we formulated the joint transmit and jamming power allocation problem as a NBG to maximize the user's covert rate with limited transmit and jamming power and ensure the covertness of communication simultaneously. To solve the formulated problem, we proposed PPA and JTPA algorithms, under the warden's optimal detection threshold. PSO was used by the warden in finding the optimal detection threshold. Furthermore, all formulated problems are proven to be convex, and the running times were investigated. Numerical results illustrated that the jammer's total power and the UAV's transmit power can be jointly allocated to improve the covert rate, and our proposed algorithms are effective. For future works, we can extend the power allocation algorithms to joint power and the three-dimension

trajectory optimization algorithms, because the UAV may fly away from the warden to weaken the detection channels.

1) Proof of PDF: Let $U_k \triangleq \frac{\gamma_k}{C_{1k}} = \frac{X_k}{T_k}$, where $T_k \triangleq \kappa^2 + C_{2k}Z_k$. The PDF of T_k can be expressed as $f_{T_k}(t) = \frac{1}{C_{2k}} f_{Z_k}\left(\frac{t-\kappa^2}{C_{2k}}\right)$. With the help of (2), we can obtain the PDF of U_k as

$$f_{U_k}(u) = \int_0^\infty x f_{X_k}(ux) f_{T_k}(x)\,\mathrm{d}x$$

$$= \frac{m_k^{m_k}}{\Gamma(m_k)} \sum_{j=0}^M \frac{K_k^j \alpha_{kj} u^j m_{fk}^{m_{fk}} (m_{sk}-1)^{m_{sk}} \bar{z}_k^{m_{sk}} I_1}{j!\Gamma(j+1)(2\sigma_k^2)^{j+1} C_{2k}^{m_{fk}} B(m_{fk}, m_{sk})}, \quad \text{(A-1)}$$

where

$$I_1 = \int_0^\infty \frac{x^{j+1}(x-\kappa^2)^{m_{fk}-1} \exp\left(-ux(2\sigma_k^2)^{-1}\right)\mathrm{d}x}{\left(m_{fk}xC_{2k}^{-1} - m_{fk}\kappa^2 C_{2k}^{-1} + (m_{sk}-1)\bar{z}_k\right)^{m_{fk}+m_{sk}}}. \quad \text{(A-2)}$$

With the help of [28, eq. (01.03.07.0001.01)], we can re-write I_1 as

$$I_1 = \frac{1}{2\pi i} \int_{\mathcal{L}_1} \Gamma(-s_1)\left(\frac{u}{2\sigma_k^2}\right)^{s_1}$$

$$\times \int_0^\infty \frac{x^{1+s_1+j}(x-\kappa^2)^{m_{fk}-1}\mathrm{d}x\mathrm{d}s_1}{\left(m_{fk}xC_{2k}^{-1} - m_{fk}\kappa^2 C_{2k}^{-1} + (m_{sk}-1)\bar{z}_k\right)^{m_{fk}+m_{sk}}}, \quad \text{(A-3)}$$

where the integration path of $\mathcal{L}_1$ goes from $\sigma_L - i\infty$ to $\sigma_L + i\infty$ and $\sigma \in \mathbb{R}$. With the help of [27, eq. (3.197.1)], [27, eq. (9.113)] and [27, eq. (8.384.1)], the integration part in (A-3) can be solved. Substituting I_1 into (A-1), after some algebraic manipulations, we further express $f_U(u)$ as (A-4), shown at the bottom of the next page.

Then, with the help of (A-4) and [29, eq. (A-1)], $f_U(u)$ can be expressed as

$$f_U(u) = \frac{m_k^{m_k}}{u\Gamma(m_k)\Gamma(m_{fk})\Gamma(m_{sk})}\left(\frac{m_{fk}\kappa^2}{\Omega_k}\right)^{m_{fk}} \sum_{j=0}^\infty \frac{K_k^j \alpha_{kj}}{\Gamma(j+1)j!}$$

$$\times H_{1,0:0,2:1,2}^{0,0:2,0:2,1}\left(\begin{array}{c|c} \frac{\kappa^2 u}{2\sigma_k^2} \\ \frac{\Omega_k}{m_{fk}\kappa^2-\Omega_k} \end{array} \begin{array}{c} (m_{fk}+m_{sk};1,1): -:(1,1) \\ -:(1+j,1)(m_{sk},1):(m_{fk},1)(m_{fk}+m_{sk},1) \end{array}\right). \quad \text{(A-5)}$$

Hence, since $f_\gamma(\gamma) = \frac{1}{C_{1k}} f_U\left(\frac{\gamma}{C_{1k}}\right)$, we can derive (10).

2) Proof of CDF: With the help of the definition of CDF, we have $F_\gamma(\gamma) = \int_0^\gamma f_\gamma(x)\,\mathrm{d}x$. Substituting (10) into the definition, the CDF of γ can be re-written as (A-6), shown at the bottom of the next page, where I_{A2} can be easily solved as $I_{A2} = \int_0^\gamma x^{s_1-1}\mathrm{d}x = \frac{1}{s_1}\gamma^{s_1} = \frac{\Gamma(s_1)}{\Gamma(s_1+1)}\gamma^{s_1}$. Substituting I_{A2} into (A-6) and using [29, eq. (A-1)], we can derive (11). The proof is completed.

A. Proof of Propositions 1

With the help of [29, eq. (A-1)], the Multivariate Fox's H-function in (11) can be expressed in the Mellin-Barnes integral form. When the interference from the jamming signal is low, i.e., $\Omega_k \to 0$, we have $\frac{\Omega_k}{m_{fk}\kappa^2-\Omega_k} \to 0$. Thus, the Mellin-Barnes integrals can be approximated by evaluating the residue at the minimum pole on the right-hand side [29, Theorem 1.11], and we have

$$F_{\gamma_k}^{LJ}(\gamma) = \frac{m_k^{m_k}}{\Gamma(m_k)}\left(\frac{m_{fk}\kappa^2}{m_{fk}\kappa^2-\Omega_k}\right)^{m_{fk}} \sum_{j=0}^\infty \frac{K_k^j \alpha_{kj}}{\Gamma(j+1)j!}$$

$$\times \frac{1}{2\pi i}\int_{\mathcal{L}_1} \frac{\Gamma(1+j+s_1)\Gamma(-s_1)}{\Gamma(1-s_1)}\left(\frac{2\sigma_k^2 C_{1k}}{\kappa^2\gamma}\right)^{s_1}\mathrm{d}s_1. \quad \text{(B-1)}$$

Using [27, eq. (9.210.1)], we obtain (13) to complete the proof.

B. Proof of Propositions 2

When the transmit power is high, i.e., $C_{1k} \to \infty$, we have $\frac{\kappa^2\gamma}{2\sigma_k^2 C_{1k}} \to 0$. Following the similar methods used in Appendix B-A, we can approximate the Mellin-Barnes integrals by evaluating the residue at the minimum pole on the right-hand side. However, $\min\{1+j, m_{sk}\}$ is different because j goes from 0 to M. Thus, when m_{sk} is not an integer, we can find j_s which satisfies $j_s + 1 < m_{sk} < j_s + 2$. When $j \in [0, j_s]$, the minimum pole is $1+j$. When $j \in [j_s+1, M]$, the minimum pole is m_{sk}. Note that when m_{sk} is an integer, we can set $j_s \triangleq m_{sk}-1$. In this case, we only need to calculate the double residue at m_{sk}. Then, we can obtain (14), which completes the proof.

C. Proof of Propositions 3

With the help of (B-1), when the transmit power is high, i.e., $\frac{\kappa^2\gamma}{2\sigma_k^2 C_{1k}} \to 0$, the Mellin-Barnes integral over $\mathcal{L}_1$ can be approximated by the similar methods in Appendix B-A. Thus, we can derive (15) to complete the proof.

For the term of $\mathbb{P}_{AF}$, we have $\mathbb{P}_{AF} = \Pr\left(\kappa^2 + C_{2w}Z_w > \varepsilon_k\right)$. Denote that $T_w \triangleq \kappa^2 + C_{2w}Z_w$, and we can derive the CDF of T_w as

$$F_{T_w}(t) = \Pr(T_w < t) = \Pr\left(\kappa^2 + C_{2w}Z_w < t\right)$$

$$= \Pr\left(Z_w < \frac{t-\kappa^2}{C_{2w}}\right) = F_{Z_w}\left(\frac{t-\kappa^2}{C_{2w}}\right), \quad \text{(C-1)}$$

$$f_U(u) = \frac{m_k^{m_k}}{u\Gamma(m_k)\Gamma(m_{fk})\Gamma(m_{sk})}\left(\frac{m_{fk}\kappa^2}{\Omega_k}\right)^{m_{fk}} \sum_{j=0}^\infty \frac{K_k^j \alpha_{kj}}{\Gamma(j+1)j!}\left(\frac{1}{2\pi i}\right)^2 \int_{\mathcal{L}_1}\int_{\mathcal{L}_2}\left(\frac{m_{fk}\kappa^2-\Omega_k}{\Omega_k}\right)^{s_2}$$

$$\times \frac{\Gamma(1+j+s_1)\Gamma(m_{sk}+s_1)\Gamma(m_{fk}+s_2)\Gamma(m_{sk}+m_{fk}+s_2)\Gamma(-s_2)}{\Gamma(m_{fk}+m_{sk}+s_1+s_2)}\left(\frac{2\sigma_k^2}{\kappa^2 u}\right)^{s_1}\mathrm{d}s_2\mathrm{d}s_1 \quad \text{(A-4)}$$

where $Z_w \triangleq h_{jw}^2$. Thus, $\mathbb{P}_{AF}$ can be expressed as

$$\mathbb{P}_{AF} = \Pr\left(\kappa^2 + C_{2w}Z_W > \varepsilon_k\right) = 1 - F_{Z_w}\left(\frac{\varepsilon_k - \kappa^2}{C_{2w}}\right)$$

$$= 1 - \frac{m_{fw}{}^{m_{fw}-1}\left(\varepsilon_k - \kappa^2\right)^{m_{fw}}}{C_{2w}{}^{m_{fw}}B(m_{fw}, m_{sw})\left(m_{sw}-1\right)^{m_{fw}}\bar{z}_w^{m_{fw}}}$$

$$\times\,{}_2F_1\left(m_{fw}, m_{fw}+m_{sw}, m_{fw}+1; -\frac{m_{fw}\left(\varepsilon_k - \kappa^2\right)}{C_{2w}\left(m_{sw}-1\right)\bar{z}_w}\right). \quad \text{(C-2)}$$

On the other hand, for the term of $\mathbb{P}_{MD}$, we have

$$\mathbb{P}_{MD} = \Pr\left(\kappa^2 + C_{1w}X_w + C_{2w}Z_w < \varepsilon_k\right) = \Pr\left(T_w + C_{1w}X_w < \varepsilon_k\right). \quad \text{(C-3)}$$

Let $Y_w = C_{1w}X_w + T_w$. The CDF of Y_w can be expressed as

$$F_{Y_w}(y) = \int_0^\infty F_{T_w}(y-t)\frac{1}{C_{1w}}f_{X_w}\left(\frac{t}{C_{1w}}\right)\mathrm{d}t. \quad \text{(C-4)}$$

Substituting (C-1) and (2) into (C-4), with the help of [27, eq. (9.113)], [27, eq. (8.331.1)] and [28, eq. (01.03.07.0001.01)], we can re-write the CDF of Y_w as (C-5), shown at the bottom of the next page.

With the help of [27, eq. (3.194.1)] and [27, eq. (8.384.1)], let $s_1 \to -t_1 - m_{fw}$ and $s_2 \to -t_2 - j - 1$. With the help of [29, eq. (A-1)], we have

$$F_{Y_w}(y) = \frac{m_w{}^{m_w}}{\Gamma(m_{fw})\Gamma(m_{sw})\Gamma(m_w)}\sum_{j=0}^{M}\frac{K_w{}^j\alpha_{wj}}{j!\,\Gamma(j+1)}$$

$$\times H_{1,0:1,3:1,1}^{0,0:3,0:1,1}\left(\begin{array}{c}\frac{\Omega_w}{m_{fw}\left(\varepsilon_{th}-\kappa^2\right)}\\\frac{2C_{1w}\sigma_w^2}{y-\kappa^2}\end{array}\middle|\begin{array}{c}(1;1,1):(1-m_{fw},1)(1,1):(-j,1)\\-:(0,1)(m_{sw},1)\,(1,1):(0,1)\end{array}\right). \quad \text{(C-6)}$$

Therefore, we can derive $\mathbb{P}_{MD}$ as $\mathbb{P}_{MD} = \Pr\left(T_w + C_{1w}X_w < \varepsilon_k\right) = F_Y(\varepsilon_k)$ to complete the proof.

APPENDIX D
PROOF OF THEOREM 2

First, the covert rate can be derived as

$$R_k = \int_0^\infty \log_2(1+\gamma)f_{\gamma_k}(\gamma)\,\mathrm{d}\gamma. \quad \text{(D-1)}$$

Substituting (10) into (D-1), we obtain the expression of R_k as (D-2), shown at the bottom of the next page, where $I_C = \int_0^\infty \log_2(1+\gamma)\gamma^{t_1-1}\mathrm{d}\gamma$.

With the help of [26, eq. (2.6.9.21)] and [27, eq. (8.334.3)], I_C can be deduced as

$$I_C = \int_0^\infty \log_2(1+\gamma)\gamma^{s_1-1}\mathrm{d}\gamma = \frac{-1}{\ln 2}\Gamma(s_1)\Gamma(-s_1). \quad \text{(D-3)}$$

Substituting (D-3) into (D-2) and using [29, eq. (A-1)], we can obtain (19), which completes the proof.

APPENDIX E
PROOF OF LEMMA 2

Using [28, eq. (01.03.07.0001.01)] and exchanging the order of integration, we can express I_L as $I_L = \frac{1}{2\pi i}\int_{\mathcal{L}}\Gamma(-s)D^s I_D ds$, where $I_D = \int_{T_1}^{T_2}t^{A+s}(B-t)^C dt$. For different cases of T_1 and T_2, I_D can be solved with the help of [27, eq. (3.194.1)], [28, eq. (06.19.07.0001.01)], [27, eq. (3.194.2)], and [27, eq. (3.191.1)] as

Cases	Results
$T_1 = 0,$ $T_2 = T$	$I_{D_1} = \frac{B^C T_2^{1+A+s}}{1+A+s}\,{}_2F_1\left(-C, 1+A+s; 2+A+s; \frac{T_2}{B}\right),$
$T_1 = T,$ $T_2 = \infty$	$I_{D_2} = \frac{B^{1+A+C+s}}{(-1)^C}B\left(\frac{B}{T_1}, -1-A-C-s, 1+C\right),$
$T_1 = 0,$ $T_2 = \infty$	$I_{D_3} = \frac{\Gamma(-1-A-C-s)}{\Gamma(-C)\Gamma^{-1}(1+A+s)}(-B)^{1+s+A}B^C,$
$T_1 = 0,$ $T_2 = B$	$I_{D_4} = \frac{\Gamma(1+C)\Gamma(1+A+s)}{\Gamma(2+A+C+s)}B^{1+s+A+C}.$

(E-1)

Substituting I_D into I_L, and using [27, eq. (9.113)], [28, eq. (06.19.07.0005.01)], [28, eq. (07.33.07.0002.01)] and [29, eq. (A-1)], we can obtain (20).

For the third case, i.e., $T_1 = 0$ and $T_2 = \infty$, we have $I_{L_3} = \Gamma(1+A)B^C(-B)^{1+A}U(1+A, 2+A+C, -BD)$, where the tricomi confluent hypergeometric function U can be approximated by [28, eq. (07.33.06.0012.01)] and [28, eq. (07.33.06.0004.01)]

$$\begin{cases}U(a,b,c) = c^{-a}\left(1+\mathcal{O}\left(\frac{1}{c}\right)\right), c \to \infty,\\U(a,b,c) = \left(\frac{\Gamma(1-b)}{\Gamma(a-b+1)} + \frac{\Gamma(b-1)}{\Gamma(a)}c^{1-b}\right)\left(1+\mathcal{O}(c)\right), c \to 0,\end{cases} \quad \text{(E-2)}$$

which completes the proof.

APPENDIX F
PROOF OF THEOREM 3

Obviously, the value of ε_k should be large, at least larger than κ^2. The reason is that the false alarm probability is always equal to 1 if $\varepsilon_k < \kappa^2$. With the help of [27, eq. (9.100)] and (C-5), taking the second order derivative of ξ_k, we obtain (F-1), shown at the bottom of the next page.

$$F_\gamma(\gamma)\frac{m_k{}^{m_k}}{\Gamma(m_k)\Gamma(m_{fk})\Gamma(m_{sk})}\left(\frac{m_{fk}\kappa^2}{\Omega_k}\right)^{m_{fk}}\sum_{j=0}^{\infty}\frac{K_k{}^j\alpha_{kj}}{\Gamma(j+1)j!}\left(\frac{1}{2\pi i}\right)^2\int_{\mathcal{L}_1}\int_{\mathcal{L}_2}I_{A_2}\left(\frac{\Omega_k}{m_{fk}\kappa^2 - \Omega_k}\right)^{s_2}$$

$$\times\frac{\Gamma(1+j-s_1)\Gamma(m_{sk}-s_1)\Gamma(m_{fk}-s_2)\Gamma(m_{sk}+m_{fk}-s_2)\Gamma(s_2)}{\Gamma(m_{fk}+m_{sk}-s_1-s_2)}\left(\frac{\kappa^2}{2\sigma_k^2}\frac{1}{C_{1k}}\right)^{s_1}\mathrm{d}s_2\mathrm{d}s_1 \quad \text{(A-6)}$$

$$F_{Y_w}(y) = \frac{\Gamma^{-1}(m_{fw}+m_{sw})m_{fw}{}^{m_{fw}}}{C_{2w}{}^{m_{fw}}B(m_{fw}, m_{sw})(m_{sw}-1)^{m_{fw}}\bar{z}_w^{m_{fw}}}\frac{m_w{}^{m_w}}{\Gamma(m_w)}\sum_{j=0}^{\infty}\frac{K_w{}^j\alpha_{wj}}{j!\,\Gamma(j+1)(2C_{1w}\sigma_w^2)^{j+1}}\left(\frac{1}{2\pi i}\right)^2$$

$$\times\int_{\mathcal{L}_1}\int_{\mathcal{L}_2}\frac{\Gamma(m_{fw}+s_1)\Gamma(m_{fw}+m_{sw}+s_1)\Gamma(-s_1)}{\Gamma(m_{fw}+1+s_1)\Gamma^{-1}(-s_2)}\left(\frac{m_{fw}}{\Omega_w}\right)^{s_1}\left(\frac{1}{2C_{1w}\sigma_w^2}\right)^{s_2}\int_0^\infty t^{j+s_2}\left(y-t-\kappa^2\right)^{s_1+m_{fw}}\mathrm{d}t\mathrm{d}s_2\mathrm{d}s_1 \quad \text{(C-5)}$$

In the following, we aim to prove that $\frac{\partial^2 \xi_k}{\partial \varepsilon_k^2} > 0$ for any q. After some algebraic manipulations, we only need to prove

$$\frac{m_w{}^{m_w}}{\Gamma(m_w)} \sum_{j=0}^{\infty} \frac{\Gamma^{-1}(j+1) K_w{}^j \alpha_{wj} I_E}{j!(2C_{1w}\sigma_w^2)^{j+1}} > \left(\varepsilon_{th} - \kappa^2\right)^{q+m_{fw}-2}, \quad \text{(F-2)}$$

where $I_E = \int_0^{\infty} t^j \left(\varepsilon_k - \kappa^2 - t\right)^{q+m_{fw}-2} \exp\left(-\frac{t}{2C_{1w}\sigma_w^2}\right) dt$. Let T_E denote a constant, where $T_E \in \left(0, \varepsilon_k - \kappa^2\right)$. Because $t^j \left(\varepsilon_k - \kappa^2 - t\right)^{q+m_{fw}-2} \exp\left(-\frac{t}{2C_{1w}\sigma_w^2}\right) > 0$ when $t < \varepsilon_k - \kappa^2$, we have

$$I_1 > \int_{T_E}^{\infty} t^j \left(\varepsilon_k - \kappa^2 - t\right)^{q+m_{fw}-2} \exp\left(-\frac{t}{2C_{1w}\sigma_w^2}\right) dt. \quad \text{(F-3)}$$

With the help of Lemma 2, when T_E is close to zero, we only need to prove that

$$\frac{m_w{}^{m_w}}{\Gamma(m_w)} \sum_{j=0}^{M} \frac{K_w{}^j \alpha_{wj}}{j!} \left(\varepsilon_k - \kappa^2\right)^{q+m_{fw}-2} \geqslant \left(\varepsilon_{th} - \kappa^2\right)^{q+m_{fw}-2}. \quad \text{(F-4)}$$

Obviously, (F-4) is correct because $\frac{m_w{}^{m_w}}{\Gamma(m_w)} \sum_{j=0}^{M} \frac{K_w{}^j \alpha_{wj}}{j!} = 1$. Thus, we conclude that the detection error probability is convex with respect to ε_k.

APPENDIX G
PROOF OF THEOREM 4

Following the similar methods in Appendix F, we can express the second order derivative of ξ_k as (G-1), shown at the bottom of the next page.

With the help of [27, eq. (3.383.1)], [27, eq. (8.384.1)], and [28, eq. (07.20.07.0004.01)], after some algebraic manipulations, proving $\frac{\partial^2 \xi_k}{\partial C_{2w}^2} < 0$ is equivalent to prove that

$$F_2(C_{1w}) \triangleq \frac{m_w{}^{m_w}}{\Gamma(m_w)} \sum_{j=0}^{M} \frac{K_w{}^j \alpha_{wj} \Gamma(m_w+q+1)}{j! \Gamma(j+1)} \frac{1}{2\pi i}$$
$$\times \int_{\mathcal{L}} \frac{\Gamma(t+j+1)\Gamma(-t)}{\Gamma(m_w+q+1-t)} \left(\frac{2C_{1w}\sigma_w^2}{\varepsilon_k^{opt} - \kappa^2}\right)^t dt < 1, \quad \text{(G-2)}$$

where the integration path of $\mathcal{L}$ goes from $\sigma_L - i\infty$ to $\sigma_L + i\infty$ and $\sigma \in \mathbb{R}$. When $C_{1w} \to \infty$, we have

$$F_2(C_{1w}) \approx \frac{m_w{}^{m_w}}{\Gamma(m_w)} \sum_{j=0}^{M} \frac{K_w{}^j \alpha_{wj} \Gamma(m_w+q+1)}{j! \Gamma(m_w+q+2+j)} \left(\frac{\varepsilon_k^{opt} - \kappa^2}{2C_{1w}\sigma_w^2}\right)^{j+1} \to 0, \quad \text{(G-3)}$$

which means that there must exist C_{1w}' such that when C_{1w} is greater than C_{1w}', we always have $\frac{\partial^2 \xi_k}{\partial C_{2w}^2} < 0$. This is reasonable because the UAV transmit power allocated to users should be large enough to meet the QoS requirements. Users may quit gaming if their data rate is too low.

To obtain $\frac{\partial^2 \xi_k}{\partial C_{1w}\partial C_{2w}}$, $\frac{\partial^2 \xi_k}{\partial C_{2w}\partial C_{1w}}$ and $\frac{\partial^2 \xi_k}{\partial C_{1w}^2}$, with the help of Appendix E, we can rewrite ξ_k as (G-4), shown at the bottom of the next page, where $I_J = \int_0^{\infty} t^{j+p} \left(\varepsilon_k - \kappa^2 - t\right)^{q+m_{fw}} dt$. With the help of (G-4), we can obtain

$$\frac{\partial^2 \xi_k}{\partial C_{1w}^2} = \frac{m_w{}^{m_w} \Gamma^{-1}(m_w) m_{fw}{}^{m_{fw}-1} \bar{z}_w^{-m_{fw}}}{B(m_{fw}, m_{sw})(m_{sw}-1)^{m_{fw}}} I_J$$
$$\times \sum_{j=0}^{\infty} \frac{\Gamma^{-1}(j+1) K_w{}^j \alpha_{wj}}{j!(2\sigma_w^2)^{j+1}} \sum_{p=0}^{\infty} \sum_{q=0}^{\infty} \frac{(m_{fw})_q (m_{fw}+m_{sw})_q}{(m_{fw}+1)_q q!}$$
$$\times \frac{1}{p!} \left(\frac{-1}{2\sigma_w^2}\right)^p \left(\frac{-m_{fw}}{(m_{sw}-1)\bar{z}_w}\right)^q \frac{(p+j+1)(p+j+2)}{C_{1w}^{p+j+3} C_{2w}^{q+m_{fw}}}, \quad \text{(G-5)}$$

and

$$\frac{\partial^2 \xi_k}{\partial C_{1w}\partial C_{2w}} = \frac{\partial^2 \xi_k}{\partial C_{2w}\partial C_{1w}} = \frac{I_J \bar{z}_w^{-m_{fw}} m_{fw}{}^{m_{fw}-1}}{B(m_{fw}, m_{sw})(m_{sw}-1)^{m_{fw}}}$$
$$\times \frac{m_w{}^{m_w}}{\Gamma(m_w)} \sum_{j=0}^{\infty} \frac{K_w{}^j \alpha_{wj}}{j! \Gamma(j+1)(2\sigma_w^2)^{j+1}} \sum_{p=0}^{\infty} \frac{1}{p!} \left(\frac{-1}{2\sigma_w^2}\right)^p$$
$$\times \sum_{q=0}^{\infty} \frac{(m_{fw})_q (m_{fw}+m_{sw})_q}{(m_{fw}+1)_q q!} \left(\frac{\bar{z}_w^{-1} m_{fw}}{1-m_{sw}}\right)^q \frac{p+j+1}{C_{1w}^{p+j+2}} \frac{q+m_{fw}}{C_{2w}^{q+m_{fw}+1}}. \quad \text{(G-6)}$$

Comparing (G-5) and (G-6) with (G-4), we can conclude that $\frac{\partial^2 \xi_k}{\partial C_{1w}\partial C_{2w}} \times \frac{\partial^2 \xi_k}{\partial C_{2w}\partial C_{1w}} > 0$ and $\frac{\partial^2 \xi_k}{\partial C_{1w}^2} > 0$. Thus, we have $\nabla^2 \xi_k = \frac{\partial^2 \xi_k}{\partial C_{1w}^2} \frac{\partial^2 \xi_k}{\partial C_{2w}^2} - \frac{\partial^2 \xi_k}{\partial C_{1w}\partial C_{2w}} \frac{\partial^2 \xi_k}{\partial C_{2w}\partial C_{1w}} < 0$, which completes the proof.

REFERENCES

[1] X. Zhou, S. Yan, D. W. K. Ng, and R. Schober, "Three-Dimensional placement and transmit power design for UAV covert communications,"

$$R_k = \frac{m_k{}^{m_k}}{\Gamma(m_k)\Gamma(m_{fk})\Gamma(m_{sk})} \left(\frac{m_{fk}\kappa^2}{\Omega_k}\right)^{m_{fk}} \sum_{j=0}^{\infty} \frac{K_k{}^j \alpha_{kj}}{\Gamma(j+1) j!} \left(\frac{1}{2\pi i}\right)^2 \int_{\mathcal{L}_1} \int_{\mathcal{L}_2} \left(\frac{\Omega_k}{m_{fk}\kappa^2 - \Omega_k}\right)^{s_2}$$
$$\times \frac{\Gamma(1+j-s_1)\Gamma(m_{sk}-s_1)\Gamma(m_{fk}-s_2)\Gamma(m_{sk}+m_{fk}-s_2)\Gamma(s_2)}{\Gamma(m_{fk}+m_{sk}-s_1-s_2)} \left(\frac{\kappa^2}{2\sigma_k^2} \frac{1}{C_{1k}}\right)^{s_1} I_C ds_2 ds_1, \quad \text{(D-2)}$$

$$\frac{\partial^2 \xi_k}{\partial \varepsilon_{th}^2} = \frac{m_{fw}{}^{m_{fw}-1}}{C_4{}^{m_{fw}} B(m_{fw}, m_{sw})(m_{sw}-1)\bar{z}_w^{m_{fw}}} \frac{m_w{}^{m_w}}{\Gamma(m_w)} \sum_{j=0}^{\infty} \frac{K_w{}^j \alpha_{wj}}{j!} \frac{(q+m_{fw})(q+m_{fw}-1)}{\Gamma(j+1)(2C_3\sigma_w^2)^{j+1}}$$
$$\times \int_0^{\infty} t^j \left(\varepsilon_{th} - \kappa^2 - t\right)^{m_{fw}} \exp\left(-\frac{t}{2C_3\sigma_w^2}\right) \sum_{q=0}^{\infty} \frac{(m_{fw})_q (m_{fw}+m_{sw})_q}{(m_{fw}+1)_q q!} \left(-\frac{m_{fw}(\varepsilon_{th} - t - \kappa^2)}{C_4(m_{sw}-1)\bar{z}_w}\right)^q dt$$
$$- \frac{(q+m_{fw})(q+m_{fw}-1)(\varepsilon_{th} - \kappa^2)^{m_{fw}-2} m_{fw}{}^{m_{fw}-1}}{C_4{}^{m_{fw}} B(m_{fw}, m_{sw})(m_{sw}-1)\bar{z}_w^{m_{fw}}} \sum_{q=0}^{\infty} \frac{(m_{fw})_q (m_{fw}+m_{sw})_q}{(m_{fw}+1)_q q!} \left(-\frac{m_{fw}(\varepsilon_{th} - \kappa^2)}{C_4(m_{sw}-1)\bar{z}_w}\right)^q \quad \text{(F-1)}$$

IEEE Trans. Veh. Technol., vol. 70, no. 12, pp. 13 424–13 429, Dec. 2021.

[2] B. Li, Z. Fei, Y. Zhang, and M. Guizani, "Secure UAV communication networks over 5G," *IEEE Wireless Commun.*, vol. 26, no. 5, pp. 114–120, may. 2019.

[3] Z. Lin, M. Lin, T. de Cola, J.-B. Wang, W.-P. Zhu, and J. Cheng, "Supporting IoT with rate-splitting multiple access in satellite and aerial-integrated networks," *IEEE Internet Things J.*, vol. 8, no. 14, pp. 11 123–11 134, Jan. 2021.

[4] P. X. Nguyen, V.-D. Nguyen, H. V. Nguyen, and O.-S. Shin, "Uav-assisted secure communications in terrestrial cognitive radio networks: Joint power control and 3D trajectory optimization," *IEEE Trans. Veh. Technol.*, vol. 70, no. 4, pp. 3298–3313, Apr. 2021.

[5] M. Cui, G. Zhang, Q. Wu, and D. W. K. Ng, "Robust trajectory and transmit power design for secure UAV communications," *IEEE Trans. Veh. Technol.*, vol. 67, no. 9, pp. 9042–9046, Sept. 2018.

[6] B. Yang, T. Taleb, Y. Shen, X. Jiang, and W. Yang, "Performance, fairness, and tradeoff in UAV swarm underlaid mmWave cellular networks with directional antennas," *IEEE Trans. Wireless Commun.*, vol. 20, no. 4, pp. 2383–2397, Apr. 2021.

[7] L. Zhu, J. Zhang, Z. Xiao, X. Cao, X.-G. Xia, and R. Schober, "Millimeter-wave full-duplex UAV relay: Joint positioning, beamforming, and power control," *IEEE J. Sel. Areas Commun.*, vol. 38, no. 9, pp. 2057–2073, Sept. 2020.

[8] X. Jiang, X. Chen, J. Tang, N. Zhao, X. Y. Zhang, D. Niyato, and K.-K. Wong, "Covert communication in UAV-assisted air-ground networks," *IEEE Wireless Commun.*, vol. 28, no. 4, pp. 190–197, Aug. 2021.

[9] X. Chen, W. Sun, C. Xing, N. Zhao, Y. Chen, F. R. Yu, and A. Nallanathan, "Multi-antenna covert communication via Full-Duplex jamming against a warden with uncertain locations," *IEEE Trans. Wireless Commun.*, vol. 20, no. 8, pp. 5467–5480, Aug. 2021.

[10] X. Jiang, Z. Yang, N. Zhao, Y. Chen, Z. Ding, and X. Wang, "Resource allocation and trajectory optimization for UAV-enabled multi-user covert communications," *IEEE Trans. Veh. Technol.*, vol. 70, no. 2, pp. 1989–1994, Feb. 2021.

[11] J. Zhang, X. Chen, M. Li, and M. Zhao, "Optimized throughput in covert millimeter-wave UAV communications with beam sweeping," *IEEE Wireless Commun. Lett.*, vol. 10, no. 4, pp. 720–724, Apr. 2020.

[12] K. Shahzad, X. Zhou, S. Yan, J. Hu, F. Shu, and J. Li, "Achieving covert wireless communications using a Full-Duplex receiver," *IEEE Trans. Wireless Commun.*, vol. 17, no. 12, pp. 8517–8530, Dec. 2018.

[13] K. Yoon, D. Park, Y. Yim, K. Kim, S. K. Yang, and M. Robinson, "Security authentication system using encrypted channel on UAV network," in *Proc. IEEE Int. Conf. Robot. Comput.*, Apr. 2017, pp. 393–398.

[14] S. Atoev, O.-J. Kwon, C.-Y. Kim, S.-H. Lee, Y.-R. Choi, and K.-R. Kwon, "The secure UAV communication link based on OTP encryption technique," in *Proc. 11th Int. Conf. Ubiquitous Future Netw. (ICUFN)*, Jul. 2019, pp. 1–3.

[15] G. Zhang, Q. Wu, M. Cui, and R. Zhang, "Securing UAV communications via joint trajectory and power control," *IEEE Trans. Wireless Commun.*, vol. 18, no. 2, pp. 1376–1389, Feb. 2019.

[16] L. Zhou, D. Wu, X. Wei, and Z. Dong, "Seeing isn't believing: QoE evaluation for privacy-aware users," *IEEE J. Sel. Areas Commun.*, vol. 37, no. 7, pp. 1656–1665, Jul. 2019.

[17] Y. Wang, S. Yan, W. Yang, Y. Huang, and C. Liu, "Energy-efficient covert communications for bistatic backscatter systems," *IEEE Trans. Veh. Technol.*, vol. 70, no. 3, pp. 2906–2911, Mar. 2021.

[18] M. J. Osborne and A. Rubinstein, *A course in game theory*. MIT press, 1994.

[19] Z. Han, D. Niyato, W. Saad, T. Başar, and A. Hjørungnes, *Game theory in wireless and communication networks: Theory, models, and applications*. Cambridge university press, 2012.

[20] Z. Zheng, L. Song, D. Niyato, and Z. Han, "Resource allocation in wireless powered relay networks: A bargaining game approach," *IEEE Trans. Veh. Technol.*, vol. 66, no. 7, pp. 6310–6323, Jul. 2016.

[21] J. F. Nash, "The bargaining problem," *Econometrica, J. Econ. Soc.*, vol. 18, no. 2, pp. 155–162, 1950.

[22] S. K. Yoo, S. L. Cotton, P. C. Sofotasios, M. Matthaiou, M. Valkama, and G. K. Karagiannidis, "The Fishe-Snedecor $\mathcal{F}$ distribution: A simple and accurate composite fading model," *IEEE Commun. Lett.*, vol. 21, no. 7, pp. 1661–1664, Jul. 2017.

[23] J. Zhang, W. Zeng, X. Li, Q. Sun, and K. P. Peppas, "New results on the fluctuating two-ray model with arbitrary fading parameters and its applications," *IEEE Trans. Veh. Technol.*, vol. 67, no. 3, pp. 2766–2770, Mar. 2017.

[24] Y. Cheng, K. H. Li, Y. Liu, K. C. Teh, and H. V. Poor, "Downlink and uplink intelligent reflecting surface aided networks: NOMA and OMA," *IEEE Trans. Wireless Commun.*, vol. 20, no. 6, pp. 3988–4000, Jun. 2021.

[25] P. Liu, D. Kong, J. Ding, Y. Zhang, K. Wang, and J. Choi, "Channel estimation aware performance analysis for massive MIMO with Rician fading," *IEEE Trans. Commun.*, vol. 69, no. 7, pp. 4373–4386, Jul. 2021.

[26] A. P. Prudnikov, J. A. Bryčkov, and O. I. Maričev, *Integrals and Series. Vol. 1, Elementary Function*, 1986.

[27] I. S. Gradshteyn and I. M. Ryzhik, *Table of Integrals, Series, and Products*, 7th ed. Academic Press, 2007.

[28] Wolfram, "The wolfram functions site," http://functions.wolfram.com.

[29] A. M. Mathai, R. K. Saxena, and H. J. Haubold, *The H-function: Theory and Applications*. Springer Science & Business Media, 2009.

[30] J. Zhang, H. Du, P. Zhang, J. Cheng, and L. Yang, "Performance analysis of 5G mobile relay systems for high-speed trains," *IEEE J. Select. Areas Commun.*, vol. 38, no. 12, pp. 2760–2772, Dec. 2020.

[31] M. R. Akdeniz, Y. Liu, M. K. Samimi, S. Sun, S. Rangan, T. S. Rappaport, and E. Erkip, "Millimeter wave channel modeling and cellular capacity evaluation," *IEEE J. Sel. Areas Commun.*, vol. 32, no. 6, pp. 1164–1179, Jun. 2014.

[32] K. Rabie, B. Adebisi, G. Nauryzbayev, O. S. Badarneh, X. Li, and M.-S. Alouini, "Full-Duplex energy-harvesting enabled relay networks in generalized fading channels," *IEEE Wireless Commun. Lett.*, vol. 8, no. 2, pp. 384–387, Apr. 2019.

[33] H. Du, J. Zhang, K. P. Peppas, H. Zhao, B. Ai, and X. Zhang, "On the distribution of the ratio of products of Fisher-Snedecor $\mathcal{F}$ random

$$\frac{\partial^2 \xi_k}{\partial C_{2w}^2} = \frac{(q+m_{fw})(1+q+m_{fw})m_{fw}^{m_{fw}-1}}{C_{2w}^{q+m_{fw}+2}B(m_{fw},m_{sw})(m_{sw}-1)^{m_{fw}}\bar{z}_w^{m_{fw}}}\frac{m_w^{m_w}}{\Gamma(m_w)}\sum_{j=0}^{M}\frac{K_w^j\alpha_{wj}}{j!}\frac{1}{\Gamma(j+1)(2C_{1w}\sigma_w^2)^{j+1}}$$
$$\times \int_0^\infty t^j\left(\varepsilon_k^{opt}-\kappa^2-t\right)^{m_{fw}}\exp\left(\frac{-t}{2C_{1w}\sigma_w^2}\right)\sum_{q=0}^{\infty}\frac{(m_{fw})_q(m_{fw}+m_{sw})_q}{(m_{fw}+1)_q q!}\left(-\frac{m_{fw}\left(\varepsilon_k^{opt}-t-\kappa^2\right)}{(m_{sw}-1)\bar{z}_w}\right)^q \mathrm{d}t$$
$$-\frac{(q+m_{fw})(1+q+m_{fw})m_{fw}^{m_{fw}-1}\left(\varepsilon_k^{opt}-\kappa^2\right)^{m_{fw}}}{C_{2w}^{q+m_{fw}+2}B(m_{fw},m_{sw})(m_{sw}-1)^{m_{fw}}\bar{z}_w^{m_{fw}}}\sum_{q=0}^{\infty}\frac{(m_{fw})_q(m_{fw}+m_{sw})_q}{(m_{fw}+1)_q q!}\left(-\frac{m_{fw}\left(\varepsilon_k^{opt}-\kappa^2\right)}{(m_{sw}-1)\bar{z}_w}\right)^q \quad \text{(G-1)}$$

$$\xi_k = 1 - \frac{m_{fw}^{m_{fw}-1}\left(\varepsilon_k-\kappa^2\right)^{m_{fw}}}{B(m_{fw},m_{sw})(m_{sw}-1)^{m_{fw}}\bar{z}_w^{m_{fw}}}\sum_{q=0}^{\infty}\frac{(m_{fw})_q(m_{fw}+m_{sw})_q}{(m_{fw}+1)_q q!}\left(\frac{m_{fw}\left(\varepsilon_k-\kappa^2\right)}{(1-m_{sw})\bar{z}_w}\right)^q\frac{1}{C_{2w}^{q+m_{fw}}}+\frac{m_{fw}^{m_{fw}-1}\bar{z}_w^{-m_{fw}}}{B(m_{fw},m_{sw})(m_{sw}-1)^{m_{fw}}}$$
$$\times\frac{m_w^{m_w}}{\Gamma(m_w)}\sum_{j=0}^{\infty}\frac{K_w^j\alpha_{wj}}{j!}\frac{1}{\Gamma(j+1)(2\sigma_w^2)^{j+1}}\sum_{p=0}^{\infty}\frac{1}{p!}\left(\frac{-1}{2\sigma_w^2}\right)^p\sum_{q=0}^{\infty}\frac{(m_{fw})_q(m_{fw}+m_{sw})_q}{(m_{fw}+1)_q q!}\left(\frac{-m_{fw}}{(m_{sw}-1)\bar{z}_w}\right)^q\frac{1}{C_{1w}^{p+j+1}}\frac{1}{C_{2w}^{q+m_{fw}}}I_J \quad \text{(G-4)}$$

variables and its applications," *IEEE Trans. Veh. Technol.*, vol. 69, no. 2, pp. 1855–1866, Feb. 2020.

[34] J. M. Romero-Jerez, F. J. Lopez-Martinez, J. F. Paris, and A. J. Goldsmith, "The fluctuating two-ray fading model: Statistical characterization and performance analysis," *IEEE Trans. Wireless Commun.*, vol. 16, no. 7, pp. 4420–4432, Jul. 2017.

[35] J. Zheng, J. Zhang, G. Pan, J. Cheng, and B. Ai, "Sum of squared fluctuating two-ray random variables with wireless applications," *IEEE Trans. Veh. Technol.*, vol. 68, no. 8, pp. 8173–8177, Aug. 2019.

[36] S. K. Yoo, P. C. Sofotasios, S. L. Cotton, S. Muhaidat, F. J. Lopez-Martinez, J. M. Romero-Jerez, and G. K. Karagiannidis, "A comprehensive analysis of the achievable channel capacity in $\mathcal{F}$ composite fading channels," *IEEE Access*, vol. 7, pp. 34 078 –34 094, Mar. 2019.

[37] K.-W. Huang, H. Deng, and H.-M. Wang, "Jamming aided covert communication with multiple receivers," *IEEE Trans. Wireless Commun.*, vol. 20, no. 7, pp. 4480–4494, Jul. 2021.

[38] H. Du, J. Zhang, J. Cheng, and B. Ai, "Millimeter wave communications with reconfigurable intelligent surfaces: Performance analysis and optimization," *IEEE Trans. Commun.*, vol. 69, no. 4, pp. 2752–2768, Apr. 2021.

[39] X. Zhou, S. Yan, J. Hu, J. Sun, J. Li, and F. Shu, "Joint optimization of a UAV's trajectory and transmit power for covert communications," *IEEE Trans. Signal Process.*, vol. 67, no. 16, pp. 4276–4290, Aug. 2019.

[40] R. Soltani, D. Goeckel, D. Towsley, B. A. Bash, and S. Guha, "Covert wireless communication with artificial noise generation," *IEEE Trans. Wireless Commun.*, vol. 17, no. 11, pp. 7252–7267, Nov. 2018.

[41] J. Hu, K. Shahzad, S. Yan, X. Zhou, F. Shu, and J. Li, "Covert communications with a Full-Duplex receiver over wireless fading channels," in *Proc. IEEE ICC*, May 2018, pp. 1–6.

[42] M. Forouzesh, P. Azmi, A. Kuhestani, and P. L. Yeoh, "Joint information-theoretic secrecy and covert communication in the presence of an untrusted user and warden," *IEEE Internet Things J.*, vol. 8, no. 9, pp. 7170–7181, Sept. 2020.

[43] T. K. Lo, "Maximum ratio transmission," *IEEE Trans. Commun.*, vol. 47, no. 10, pp. 1458–1461, Oct. 1999.

[44] Y. Tokgoz and B. D. Rao, "Performance analysis of maximum ratio transmission based multi-cellular MIMO systems," *IEEE Trans. Wireless Commun.*, vol. 5, no. 1, pp. 83–89, Jan. 2006.

[45] H. Du, J. Zhang, J. Cheng, and B. Ai, "Sum of fisher-snedecor $\mathcal{F}$ random variables and its applications," *IEEE Open J. Commun. Soc.*, vol. 1, pp. 342–356, Mar. 2020.

[46] H. Buchholz, *The confluent hypergeometric function: With special emphasis on its applications*. Springer Science & Business Media, 2013, vol. 15.

[47] S. Cheng, H. Lu, X. Lei, and Y. Shi, "A quarter century of particle swarm optimization," *Complex Intell. Syst.*, vol. 4, no. 3, pp. 227–239, Mar. 2018.

[48] A. Chraibi, S. B. Alla, A. Touhafi, and A. Ezzati, "Run time optimization using a novel implementation of parallel-PSO for real-world applications," in *Proc. 5th CloudTech*, May 2020, pp. 1–7.

[49] Z. Han, Z. Ji, and K. R. Liu, "Fair multiuser channel allocation for OFDMA networks using Nash bargaining solutions and coalitions," *IEEE Trans. Commun.*, vol. 53, no. 8, pp. 1366–1376, Aug. 2005.

[50] H. Park and M. van der Schaar, "Bargaining strategies for networked multimedia resource management," *IEEE Trans. Signal Process.*, vol. 55, no. 7, pp. 3496–3511, Jul. 2007.

[51] X. Wang, S. Kwong, L. Xu, and Y. Zhang, "Generalized Nash bargaining solution to rate control optimization for spatial scalable video coding," *IEEE Trans. Image Process.*, vol. 23, no. 9, pp. 4010–4021, Sept. 2014.

[52] J. Derrac, S. García, D. Molina, and F. Herrera, "A practical tutorial on the use of nonparametric statistical tests as a methodology for comparing evolutionary and swarm intelligence algorithms," *Swarm Evol. Comput.*, vol. 1, no. 1, pp. 3–18, Jan. 2011.

[53] R. T. Rockafellar, "Lagrange multipliers and optimality," *SIAM Rev. Soc. Ind. Appl. Math*, vol. 35, no. 2, pp. 183–238, Feb. 1993.

[54] Z. Liu, K. Hou, H. Jia, J. Zhao, D. Wang, Y. Mu, and L. Zhu, "A lagrange multiplier based state enumeration reliability assessment for power systems with multiple types of loads and renewable generations," *IEEE Trans. Power Syst.*, vol. 36, no. 4, pp. 3260–3270, Apr. 2021.

[55] X. Yu, Y. Du, X. yu Dang, S.-H. Leung, and H. Wang, "Power allocation schemes for uplink massive mimo system in the presence of imperfect CSI," *IEEE Trans. Signal Process.*, vol. 68, no. 5968–5982, Oct. 2020.

[56] F. Zhang and D. R. Bull, "Rate-distortion optimization using adaptive lagrange multipliers," *IEEE Trans. Circuits Syst. Video Technol.*, vol. 29, no. 10, pp. 3121–3131, Oct. 2019.

[57] T. V. Chien, E. Bjornson, and E. G. Larsson, "Joint power allocation and load balancing optimization for energy-efficient cell-free massive MIMO networks," *IEEE Trans. Wireless Commun.*, vol. 19, no. 10, pp. 6798–6812, Oct. 2020.

Hongyang Du received the B.Sc. degree from Beijing Jiaotong University, Beijing, China, in 2021. He is currently pursuing the Ph.D. degree with the School of Computer Science and Engineering, the Energy Research Institute @ NTU, Interdisciplinary Graduate Program, Nanyang Technological University, Singapore. His research interests include Metaverse, reconfigurable intelligent surface, and communication theory.

Dusit Niyato (M'09-SM'15-F'17) is currently a professor in the School of Computer Science and Engineering, at Nanyang Technological University, Singapore. He received B.Eng. from King Mongkuts Institute of Technology Ladkrabang (KMITL), Thailand in 1999 and Ph.D. in Electrical and Computer Engineering from the University of Manitoba, Canada in 2008. His research interests are in the areas of Internet of Things (IoT), machine learning, and incentive mechanism design.

Yuan-Ai Xie received the B.S. degree in automation from North China University of Science and Technology, Tangshan, China, in 2016. He is currently pursuing the Ph.D. degree in control science and engineering in Yanshan University, Qinhuangdao, China. His current research interests include wireless resource optimization in vehicular network and covert communication.

Yanyu Cheng (Member, IEEE) received the B.Eng. degree in information engineering from Shanghai Jiao Tong University, Shanghai, China, in 2015, and the M.Sc. degree in signal processing and the Ph.D. degree in electrical engineering from Nanyang Technological University (NTU), Singapore, in 2016 and 2021, respectively. He is currently a Post-Doctoral Research Fellow with Alibaba-NTU Joint Research Institute, NTU. His research interests include 5G/6G networks, cyber security, cloud computing, and machine learning.

Jiawen Kang received the Ph.D. degree from the Guangdong University of Technology, China in 2018. He has been a postdoc at Nanyang Technological University, Singapore from 2018 to 2021. He currently is a full professor at Guangdong University of Technology, China. His research interests mainly focus on blockchain, security and privacy protection in wireless communications and networking.

Dong In Kim (Fellow, IEEE) received the Ph.D. degree in electrical engineering from the University of Southern California, Los Angeles, CA, USA, in 1990. He was a Tenured Professor with the School of Engineering Science, Simon Fraser University, Burnaby, BC, Canada. Since 2007, he has been an SKKU Fellowship Professor with the College of Information and Communication Engineering, Sungkyunkwan University (SKKU), Suwon, South Korea. He is a Fellow of the Korean Academy of Science and Technology and a Member of the National Academy of Engineering of Korea. He has been a first recipient of the NRF of Korea Engineering Research Center in Wireless Communications for RF Energy Harvesting since 2014. He has been listed as a 2020 Highly Cited Researcher by Clarivate Analytics. From 2001 to 2020, he served as an editor and an editor at large of Wireless Communications I for the IEEE Transactions on Communications. From 2002 to 2011, he also served as an editor and a Founding Area Editor of Cross-Layer Design and Optimization for the IEEE Transactions on Wireless Communications. From 2008 to 2011, he served as the Co-Editor-in-Chief for the IEEE/KICS Journal of Communications and Networks. He served as the Founding Editor-in-Chief for the IEEE Wireless Communications Letters, from 2012 to 2015. He was selected the 2019 recipient of the IEEE Communications Society Joseph LoCicero Award for Exemplary Service to Publications. He is the General Chair for IEEE ICC 2022 in Seoul.